

Uncovering Insights Into the Bio-Efficiency of *Zingiber Officinale* Roscoe: Understanding Components That Contribute Significantly to Ginger's Anti-inflammatory and Antioxidant Potential in Relationship With Modern Drying Methods

Rabiat Shola Ahmed¹, Olufemi Temitope Ademoyegun¹, Shina Salau¹, David Olamide Raphael¹

¹ Kwara State University

Funding: No specific funding was received for this work.

Potential competing interests: No potential competing interests to declare.

Abstract

This study investigates the effects of two (2) modern food drying procedures on the bioactive ability of ginger and also unlock the active ingredients responsible for their bioactivities, in an effort to uncover the interesting antioxidant and anti-inflammatory activities of ginger. These active ingredients can be the key to the development of affordable, risk-free, and efficient anti-inflammatory and anti-oxidant drugs in the future. To achieve these, the study used a diverse approach that includes in vitro metabolic research, in silico protein-ligand interactions, toxicity assessments, and molecular dynamics simulations. Results reveal that the antioxidant activity of freeze-dried ginger (FD-G) was higher than that of oven-dried ginger (OD-G). Notably, in silico analyses showed that the main chemical constituents FD-1, OD-5, and OD-7 were responsible for ginger's bioactivity by virtue of their binding affinity, structural stability, and conformational potential to the protein complex. In general, the findings could imply that dried ginger has the ability to enhance the anti-inflammatory and antioxidant activities of ginger by 12.90-17.91% and 4-11.2%, respectively, when compared to the usual drugs Vitamin C and Aspirin.

Keywords: Anti-inflammatory; Antioxidant; Bio-activity; Freeze-drying; Ginger; Molecular Dynamics; Oven-drying.

1. Introduction

Ginger (*Zingiber officinale* Roscoe) holds significant value due to its culinary, therapeutic, and economic advantages^[1]. Ginger is reported to possess therapeutic properties that aid digestion^[1], alleviate motion sickness^[2], relieve cold and flu symptoms, and reduce inflammation^[3]. To ensure a steady supply and extend the shelf life of ginger during periods of poor harvest, various traditional preservation methods are employed^[4], commonly, drying^[5]. Sun-drying is a commonly used drying technique due to its affordability and accessibility^[6]. However, modern farmers have increasingly shifted

towards the oven-drying method, as sun-drying is prone to contamination, weather dependence, and lengthy drying times [7]. Previous research indicates that sun-drying inadequately preserves the flavor and bio-active content of ginger samples, prompting the adoption of the oven-drying method [8].

Mutukiri et al., reported that while the oven-drying technique effectively preserves the shelf life and enhances the bioactive content of ginger samples compared to sun-drying, it tends to compromise the flavor and aroma due to the high temperatures involved [9]. This drawback can impede investigations into the specific phytoconstituents responsible for ginger's bioactive properties.

Another drying method yet to be widely explored for ginger is freeze drying, also known as lyophilization [10]. Freeze drying involves freezing the food substance and then removing the water content through sublimation in a vacuum environment [10], [11]. Although freeze-drying is not cost-effective, it has been reported to minimize nutrient loss through vaporization, retain sensory properties (such as taste and aroma) [9], and improve the shelf life more effectively than oven-drying and sun-drying techniques [11].

In a previous study, Mustafa et al., [7] compared the phytochemicals, antioxidants, and anti-inflammatory effects between oven-, and freeze-dried ginger extract, the study reported a broad finding that the oven dried ginger showed slightly-positive increase in antioxidant and anti-inflammatory activity of ginger than the freeze-dried method using only Gas Chromatography analytical technique and phytochemicals analysis. Unlike the in-vitro – based findings of the study by Mustafa et al., the primary objective of this study is to gain specific, molecular insight into ginger's anti-inflammatory and antioxidant properties by identifying the major compound(s) that might have contributed significantly to these activities. To accomplish this goal, the study will investigate the metabolic processes of individual compounds found in ginger. This investigation will involve analyzing their interaction with human antioxidant and anti-inflammatory genetic receptors, and evaluating their ability to bind to these genes. Additionally, the compounds will undergo toxicity screening to narrow down the selection of potential targets responsible for the observed bio-activity. Finally, Molecular Dynamics study will be employed to understand the contribution of each screened—ligand to ginger's antioxidant and anti-inflammatory activity. This study will aid in identifying the specific compound that plays the most crucial role in ginger's activity as both an antioxidant and an anti-inflammatory agent. Ultimately, the findings from this study can help guide through an alternative and cost effective route towards the development of potent anti-oxidant and anti-inflammatory drugs.

2. Methodology

2.1. Experimental methodology

2.1.1. Plant material

Fresh and matured ginger rhizomes were collected from a farm garden in Ibadan. They were authenticated by the supervisor and manager of the agricultural garden. The entire ginger rhizomes were properly washed, and drained under

running water to remove dust, grime, and sand particles. The drained rhizomes were split into three sections. The first section (RW-G) were peeled, cut into slices, and pulverized using a pestle and mortar. The second section (FD-G) were subjected to freeze-drying using freeze-dryer machine (Search Tech Instrument, UK, LGJ-10) by peeling the skin of the ginger with a knife and then cutting it into thin slices of the same size for 7 days until totally dry and crushed. And lastly, the third section were exposed to oven-drying (OV-G) for 72 h at 60°C after removing the skin of the ginger with a knife and cutting it into thin slices. The oven-dry rhizomes were ground to 20 mesh particle size before being extracted.

2.1.2. Preparation of extracts

A 5 g of each ginger sample (RW-G, OV-G, and FD-G) were mixed with 50 mL of methanol/water (80/20, v/v). After 5 minutes of stirring, the mixture was incubated in a water bath (Digital Water Bath Shaker, DK-420) at 50°C for 30 minutes. The extracts were centrifuged at 4000 r.p.m for 15 minutes (Laboratory Centrifuge KA-1000, Jiangsu, China) and filtered.

2.1.3. Determination of Total Phenolic Content (TPC)

The TPC was measured with slight modifications using the Folin-Ciocalteu reagents, as described by Lim et al.,^[3]. A 1 mL of extract was mixed with 2.5 mL of deionized water. Subsequently, a 2.5 mL of Folin-Ciocalteu reagent (10%, v/v) was added. After 5 minutes, 2 mL of Na₂CO₃ solution (7%, w/v) and 2 mL of deionized water were added. The solution was mixed homogeneously and incubated in the dark at 25°C before analysis. The absorbance was observed at $\lambda = 760$ nm using UV/Vis spectrophotometer (Double Beam, T80 series). Gallic acid was used as standard phenol with calibration curve ranging from 0 to 40 ppm. TPC was presented as mg GAE/100 g).

2.1.4. Determination of Total Flavonoid Content (TFC)

A colorimetric approach using aluminum chloride was used to calculate the TFC of the extracts, as described by Beyhan & İşleroğlu^[12] with modifications. The mixture of 1 mL of extract, 4.1 mL of distilled water, and 0.3 mL of 5% NaNO₂ was incubated for 5 minutes. A 0.6 ml of 10% AlCl₃ was then added and incubated for a further 6 minutes. A 1M NaOH (2 ml) solution and 2 ml of distilled water were then added, and the mixture was incubated for 30 minutes in the dark. At a wavelength of 510 nm, the sample's absorbance was measured. TFC was expressed as mg CE/100 g.

2.1.5. Determination of Antioxidant activity

2.1.5.1. DPPH radical scavenging activity

Following the technique reported by Gonzalez-Palma et al.,^[13] in order to assess the DPPH radical scavenging activity: In a test tube, 3.0 ml of DPPH (0.1 mM) methanolic solution was added into 0.5 ml of the extract. The control experiment substituted methanol for the extract. A UV/Vis spectrophotometer (Double Beam T80 series) was used to measure the absorbance at 517 nm following 30 minutes of incubation. This is how the DPPH-RSA was calculated:

$$\% \text{ Inhibition} = \frac{A_c - A_s}{A_c} \times 100$$

Where A_c is the absorbance of the control and A_s = Absorbance of sample

2.1.5.2. Inhibition of albumin denaturation

The anti-inflammatory activity of methanolic extracts of *Z. officinale* was investigated using the procedure developed by Kaddour et al. [14], followed by the inhibition of albumin denaturation. An equal volume of extracts was added to 1% aqueous solution of Bovine serum albumin (BSA) into a test tube. A little amount of 1N HCl was used to alter the pH of the reaction mixture. The extracts were incubated for 20 minutes at 37°C before being heated at 70°C for 5 minutes. The mixture was allowed to cool to room temperature, and the turbidity was measured at 660 nm spectrophotometrically (Double beam, T80-series). The percent inhibition of protein denaturation was calculated with the formula:

$$\% \text{ Inhibition} = \frac{A_c - A_s}{A_c} \times 100$$

Where A_c is the absorbance of the control and A_s = Absorbance of sample

2.1.6. GC-MS analysis

The Agilent 6890N gas chromatography, which has an autosampler and is coupled to a mass spectrometer, was used for this study. A one microliter of the sample was injected in the pulsed splitless mode on a fused silica column with a film thickness of 0.15 micrometers and a 30m x 0.25mm ID. The column head pressure was kept at 20 psi while helium gas was employed as the carrier gas, resulting in a constant flow rate of 1 ml/min. The column temperature was first maintained at 55 °C for 0.4 minutes, then increased to 200 °C at a rate of 25 °C per minute, then to 280 °C at a rate of 8 °C per minute, and finally to 300 °C at a rate of 25 °C per minute, kept for 2 minutes. The list of selected compounds and the comparative plots of raw, oven-, and freeze-dried ginger by virtue of their abundance from the GC-MS plot are shown in Supplementary Data 1 – 2, respectively.

2.2. Computational methodology

2.2.1. Ligand preparation

Ligands were modeled via their nomenclature obtained from the GC-MS result, using ChemDraw® Ultra version 12.0.2.1076 software [15]. Avogadro version 1.2.0 software program [16], was used to optimize the ligands to a stable conformation. The optimized ligands were saved as .SDF file extension format for further analysis and usage in the molecular docking simulations procedure.

2.2.2. Protein preparation

Receptors were sourced from the <https://www.rcsb.org> portal^[17] for further processing. The receptors were cleaned, by removing excess crystallized water, and hetero—atoms, using the BIOVIA® DS version 2021 software program^[18]. Following that, the cleaned receptor structure was saved in memory in .PDB file extension format. The receptor structure was then further optimized, polar hydrogen added, and Geister charges assigned using the Chimera® version 35.15.1443 software program^[19]. The improved receptor structure was then saved in the autodock'.PDBQT format, where it was ready for docking.

Receptor used for this study are:

1. Human Peroxiredoxin (V) (3MNG.pdb)
2. Cold-Induced Auto—inflammatory Syndrome 1 Protein (6NPY.pdb)

2.2.3. Protein-ligand interaction studies by Molecular Docking studies

The compound-Receptor interaction was carried out by a molecular docking simulation procedure using AutoDock Vina GUI software. The Autodock Vina GUI tool, version 1.2.0^[20] was used to perform molecular docking simulations in this investigation. The docking methodology consisted of verifying the protein's active site by docking known ligands retrieved from the RCSB portal. This guaranteed that the selected compounds were assessed at the receptor's active site. Based on the validation results, a box size was established for each receptor and documented in Table 1. The screening procedure was then initiated, with the determined box size for each receptor. For each simulation cycle, the exhaustiveness or run time was set to 10. The docked score was recorded and compared to the standard drug after each simulation round. This technique enabled an accurate assessment of the compounds' binding affinity as well as the identification of prospective lead compounds for further development.

Table 1. Box-Dimension used for the molecular docking simulation

Receptor	Box size Dimensions
3MNG	Center: 7.85 × 43.73 × 20.00 Dimension: 36.90 × 36.98 × 42.35
6NPY	Center: 80.32 × 99.47 × 94.69 Dimension: 36.90 × 36.99 × 42.35

2.2.4. ADMET property studies

ADMETlab version 2.0 website at <https://admetmesh.scdd.com/>^[21] was used to conduct pharmacokinetics, toxicity, and drug-likeness studies in order to predict the ADMET properties of compounds obtained from both leave and seed sample. The server calculated AMES' oral toxicity, water solubility (log S), Brain-Blood Barrier crossing (BBB), cytochrome' inhibition (CYP-450), the Lipinski rule of five^[22], and other properties as shown in Table 4. The five conditions for Lipinski violation includes: Molecular weight ≤ 500, mlogP ≤ 4.15, number of N and O ≤ 10, NH ≤ 5 and OH ≤ 5^[22].

2.2.5. Protein-ligand complex stability and conformational flexibility by Molecular Dynamics simulations

The molecular dynamics simulation for this studies were done by simulating for 100ns, of time, using the NAMD version 2.0 software. The CHARMM GUI web-server, www.charmm-gui.org [23], was used to parameterize the complexes for both the antioxidant and anti-inflammatory studies.

A Simple point charge model (SPC/E) water in a cubic box ($10 \times 10 \times 10$) Å³ was used to solve the system, leaving 5.0 nm around the solute. To neutralize all the systems, counterions in the form of K⁺ ions with a concentration of 0.15 M were set to neutralize the system using the Monté-Carlo placement method. In order to achieve a maximum force, the system's energy consumption was minimized. The system (solvated complex) were then equilibrated for a 5ns at 310 K using an isothermal-isobaric or (NPT) ensemble followed by an isothermal-isothermal or (NVT) ensemble. The electrostatic and van der Waals interaction cutoffs were set to 1.0 nm for both NVT and NPT equilibrations. The same electrostatic and van der Waals cutoffs were used for a 100 ns Molecular Dynamics simulation of these equilibrated ensembles. Visual Molecular Dynamics (VMD) version 1.9.4 [35] was used to monitor the complexes' motions and structural changes through the course of the simulation periods.

3. Results

3.1. GC-MS analysis of raw, oven-dried and freeze-dried ginger extract sample.

The Gas Chromatography Mass Spectrometer results in Supplementary Data 2 shows the peaks of identified compounds in raw, oven-, and freeze-dried ginger. Results show that regions of 14.885 to 16.774 mins show similar peaks across, raw, oven-, and freeze-dried ginger extracts. However, some prominent were found in both oven- and freeze-dried ginger but not found in raw ginger such as, 2.3 -9.486 mins and 19.662 - 21.61 mins. The selected compounds from the GC-MS results can be found in ST1.

3.2. Pythochemical screening of raw, oven-dried and freeze-dried ginger samples

The total phenolic and flavonoid contents of the extracted raw, oven-dried, and freeze-dried ginger are presented in Figure 1 and Supplementary Data 3. The results indicate that the phenolic content follows the order of RW-G (59.97 GAE/100g) < FD-G (1004.53 GAE/100g) < OD-G (1244.75 GAE/100g), showing an increasing trend. Similarly, the total flavonoid content demonstrates an increasing pattern with the order of RW-G (214.50 CE/100g) < OD-G (512.17 CE/100g) < FD-G (555.54 CE/100g).

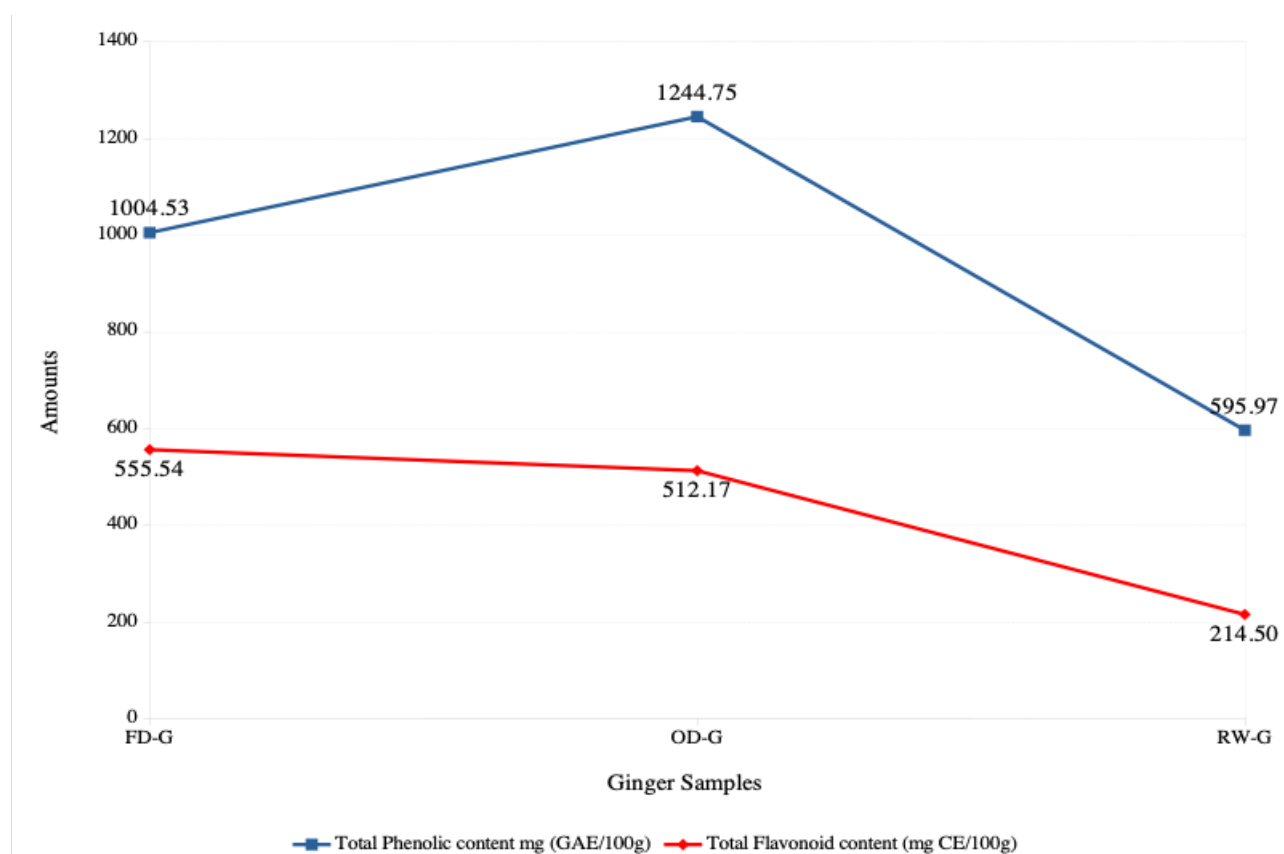


Figure 1. Total phenolic and Total flavonoid contents of the extracted Raw, Oven-dried and Freeze-dried ginger.

3.3. Analysis of antioxidant and anti-inflammatory scavenging activity

The anti-oxidant and anti-inflammatory activity of raw, oven-dried and freeze-dried ginger extracts are shown in Figure 2. Antioxidant activity results show that the DPPH radical scavenging property increases in the order of RW-G (53.12 %), OD-G (56.65 %) and FD-G (57.65 %). Likewise, the ABTS scavenging activity increases from RW-G (42.99 mg.TE/g), OD-G (63.35 mg.TE/g) and FD-G (67.30 mg.TE/g). For the Anti-inflammatory activity result, Nitric oxide scavenging activity shows increase from RW-G (35.50 %), FD-G (63.80 %) and OD-G (69.36%). Likewise for the Albumin denaturation results show a similar increase trend to nitric oxide scavenging activity such as RW-G (49.46 %), FD-G (87.51 %) and OD-G (93.21 %).

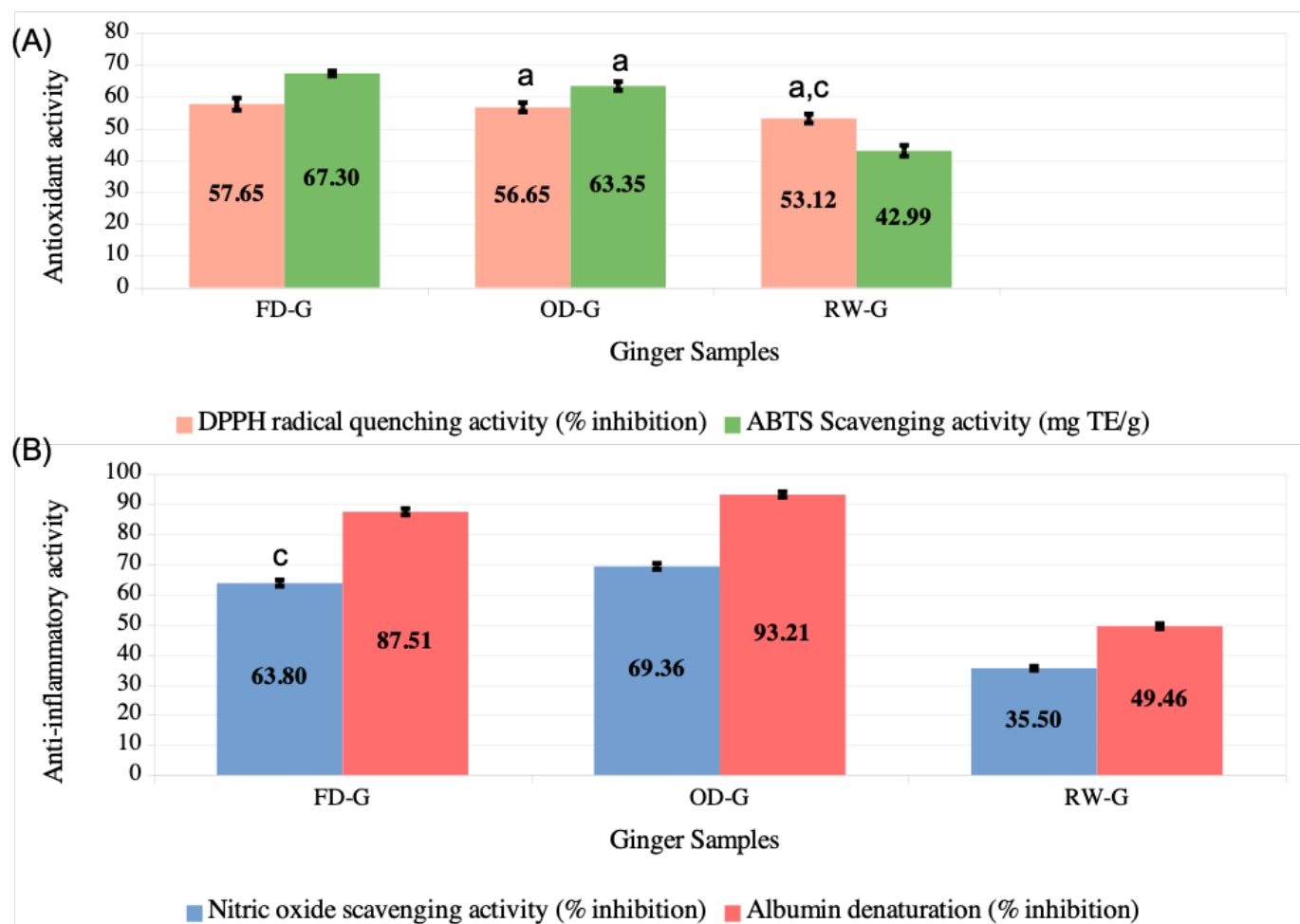


Figure 2. (A) Anti-oxidant and (B) Anti-inflammatory activity of raw, oven-dried and freeze-dried ginger extracts. [TE = Trolox Equivalent] (Means with different superscripts are significantly ($p < 0.05$) different \pm SD at $n=3$)

3.4. Protein-ligand Interactions

Compound-Receptor interaction results performed for the raw, oven-, and freeze-dried ginger are shown, both in Table 3 and Table 2, respectively, with their binding affinities (ΔG_{bind}) reported in kcal/mol.

For the anti-inflammatory studies with freeze-dried ginger, results show that FD-1 (-6.9 kcal/mol), FD-3 (-6.5 kcal/mol), FD-4 (-8.9 kcal/mol), FD-5 (-9.0 kcal/mol) and FD-6 (-7.7 kcal/mol) all cleaved better to the active site of the anti-inflammatory receptor (6NPY) compared to aspirin (-6.3 kcal/mol), the standard drug. For anti-inflammatory studies with oven-dried ginger, results show that OD-2 (-6.6 kcal/mol), OD-3 (-6.4 kcal/mol), OD-4 (-6.7 kcal/mol), OD-5 (-9.2 kcal/mol), OD-7 (-7.6 kcal/mol), OD-8 (-6.8 kcal/mol), OD-9 (-9.2 kcal/mol), and OD-10 (-8.9 kcal/mol) have better binding affinity to the active site of the anti-inflammatory receptor, (6NPY) than the standard drug, aspirin (-6.3 kcal/mol). For the anti-inflammatory studies with raw ginger, results show that RW-1 (-6.4 kcal/mol), RW-3 (-6.4 kcal/mol), RW-4—RW-6 (-6.7, -6.8, -6.7 kcal/mol respectively) RW-9 (-6.7 kcal/mol), RW-13 and RW-14 (-7.7 and -7.4 kcal/mol respectively) all cleaved better to the active site of the anti-inflammatory receptor (6NPY) compared to aspirin (-6.3 kcal/mol), the standard drug.

For the antioxidant study with freeze-dried ginger, results show that FD-4, FD-5 and FD-6 (-6.2, -6.0 and -6.0 kcal/mol respectively) binded better to the active site of the antioxidant receptor (3MNG) compared to vitamin c, the standard drug. For the antioxidant study with oven-dried ginger samples, results show that OD-2 (-5.3 kcal/mol), OD-5 (-6.6 kcal/mol), OD-7—OD-10 (-5.9, -6.1, -6.1 and -6.2 kcal/mol respectively) binded better to the active site of the antioxidant receptor (3MNG) compared to vitamin c, the standard drug. For the antioxidant study with raw-ginger, results show that, RW-9—RW-11 (-5.1, 5.1 and -5.3 kcal/mol respectively), RW-13 and RW-14 (-5.9 and -6.5 kcal/mol) binded better to the active site of the antioxidant receptor (3MNG) compared to vitamin c, the standard drug.

Table 2. Binding affinity score of anti-inflammatory and antioxidant for raw, oven-, and freeze-dried ginger ligands/compounds.

Raw Ginger				Oven-dried ginger				Freeze-dried Ginger			
Anti-inflammatory study		Antioxidant study		Anti-inflammatory study		Antioxidant study		Anti-inflammatory study		Antioxidant study	
Ligand	ΔG_{bind} (kcal/mol)	Ligand	ΔG_{bind} (kcal/mol)	Ligand	ΔG_{bind} (kcal/mol)	Ligand	ΔG_{bind} (kcal/mol)	Ligand	ΔG_{bind} (kcal/mol)	Ligand	ΔG_{bind} (kcal/mol)
*ASP	-6.3	*VTC	-4.9	OD-10	-8.9	OD-10	-6.2	FD-6	-7.7	FD-6	-6
RW-14	-7.4	RW-14	-6.5	OD-9	-9.2	OD-9	-6.1	FD-5	-9	FD-5	-6
RW-13	-7.7	RW-13	-5.9	OD-8	-6.8	OD-8	-6.1	FD-4	-8.9	FD-4	-6.2
RW-12	-6.1	RW-12	-3.6	OD-7	-7.6	OD-7	-5.9	FD-3	-6.5	FD-3	-4.3
RW-11	-6.6	RW-11	-5.3	OD-6	-6.1	OD-6	-4.2	FD-2	-5.7	FD-2	-4.8
RW-10	-6.2	RW-10	-5.1	OD-5	-9.2	OD-5	-6.6	FD-1	-6.9	FD-1	-4.7
RW-9	-6.7	RW-9	-5.1	OD-4	-6.7	OD-4	-4.8				
RW-8	-6.5	RW-8	-4.6	OD-3	-6.4	OD-3	-4.3				
RW-7	-6.2	RW-7	-4.4	OD-2	-6.6	OD-2	-5.3				
RW-6	-6.7	RW-6	-3.9	OD-1	-6.3	OD-1	-4.5				
RW-5	-6.8	RW-5	-4.3								
RW-4	-6.7	RW-4	-4.4								
RW-3	-6.4	RW-3	-4.3								
RW-2	-5.4	RW-2	-4.1								
RW-1	-6.4	RW-1	-4.2								

* Standard drugs: Aspirin® (ASP) and Vitamin C (VTC)

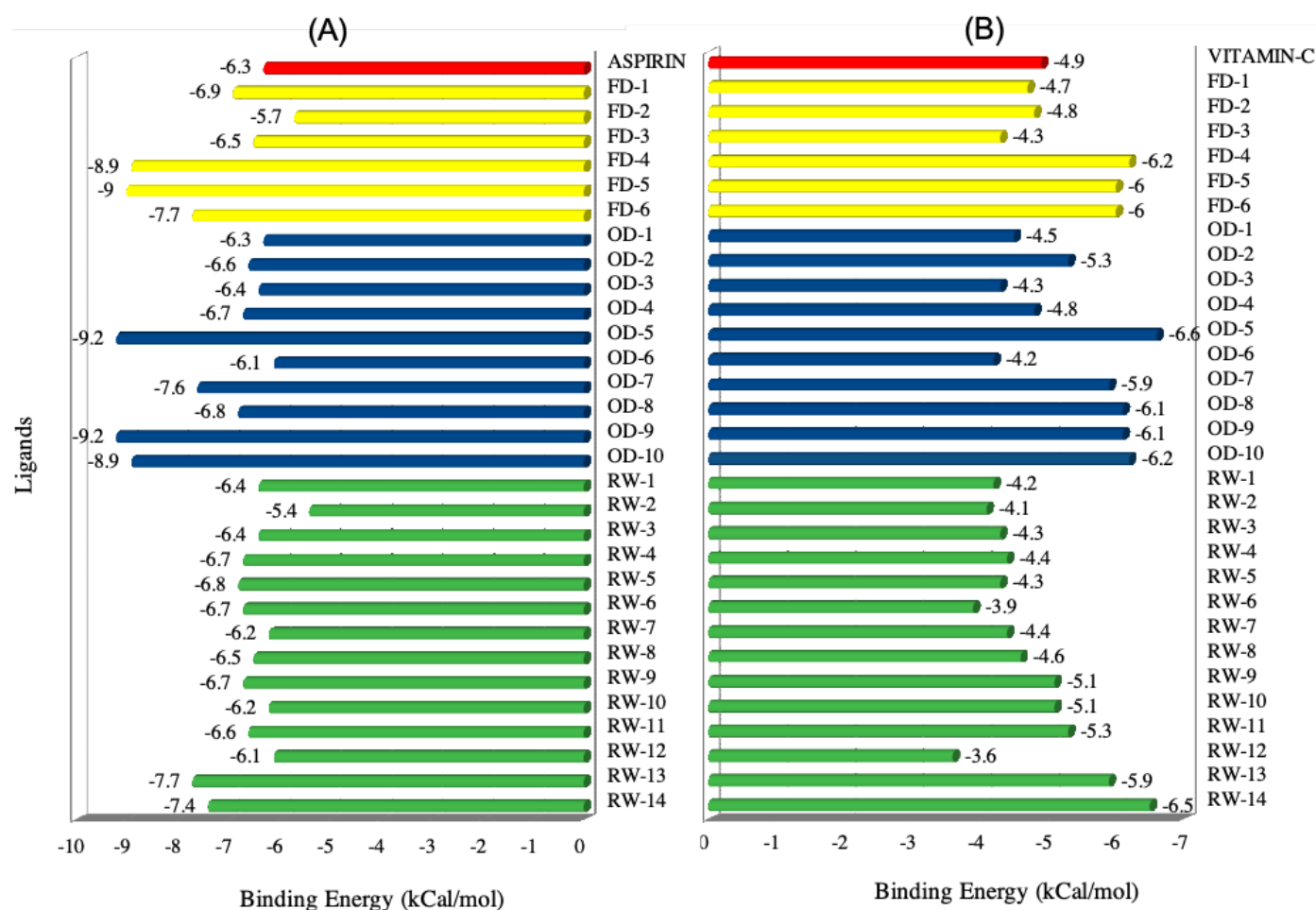
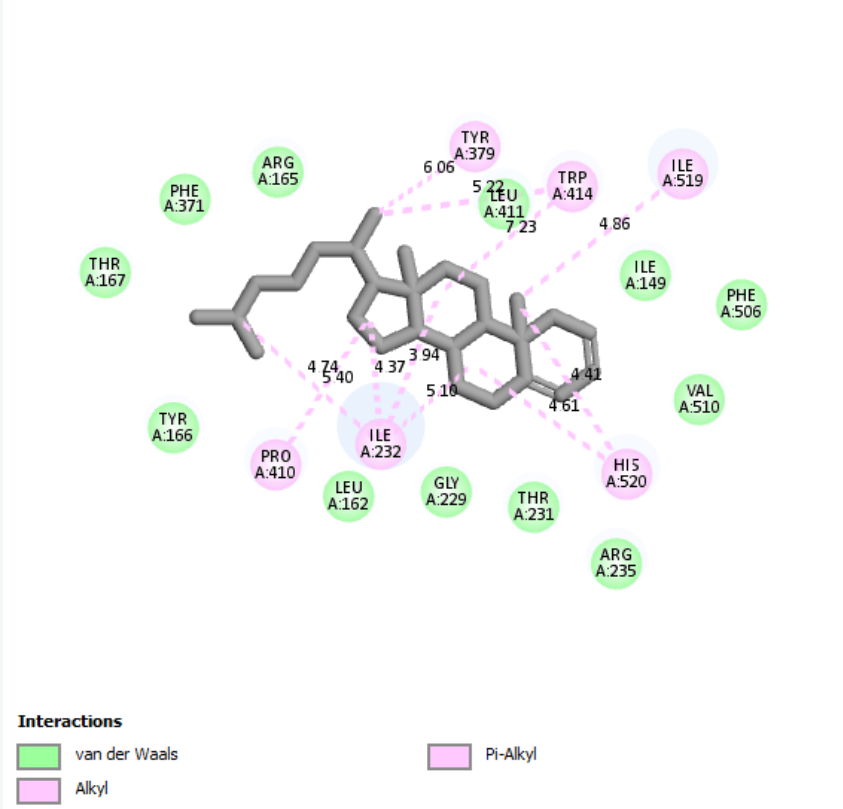
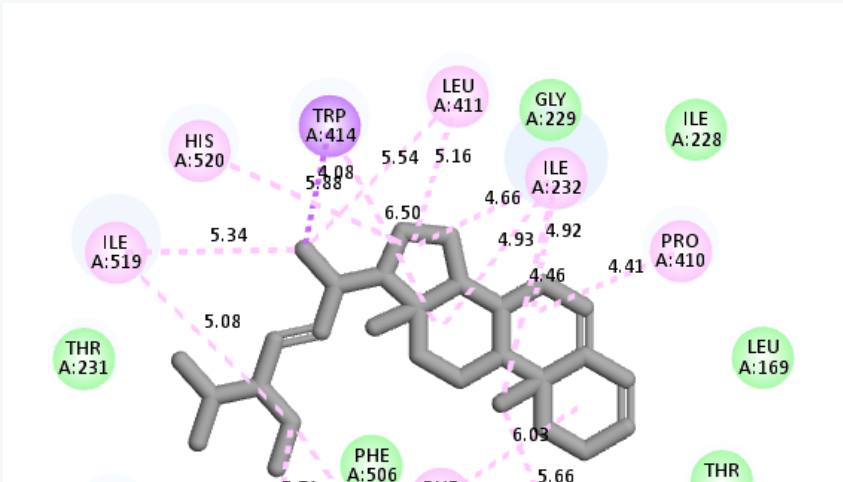


Figure 3. Binding affinity results for raw, freeze-, and oven-dried ginger extracted compounds against (A) anti-inflammatory (6NPY.pdb) and (B) antioxidant (3MNG.pdb) receptors.

Table 3. The 2D interaction of protein – ligand interaction and their bond lengths at a maximum cutoff distance of 5Å.

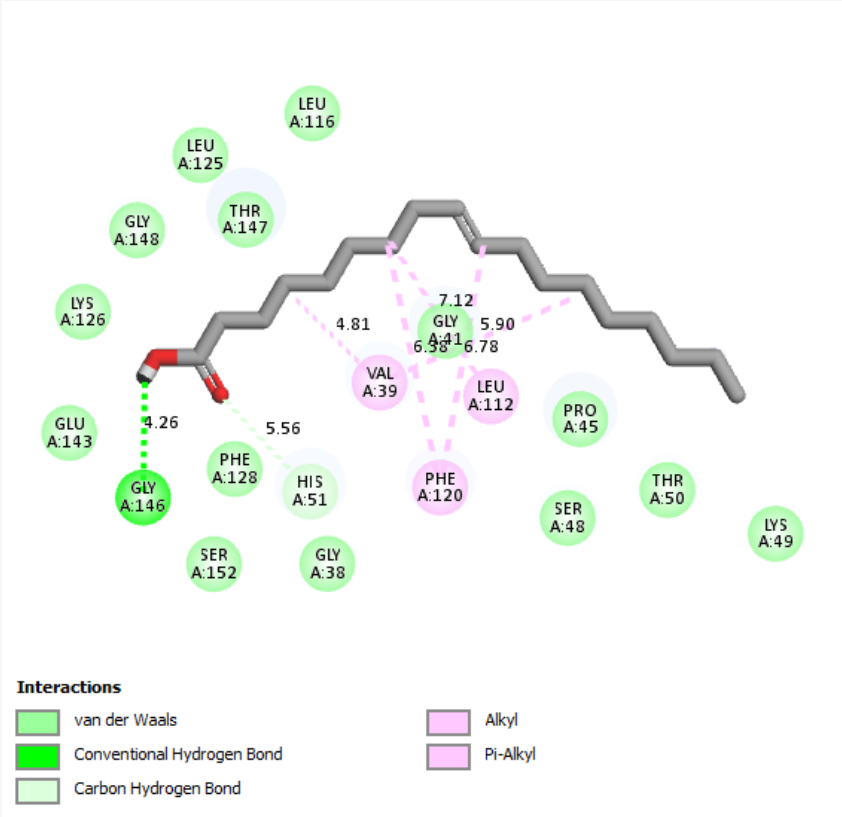
Code name	2D interaction image	Hydrogen bonds and length (Å)	Hydrophobic bonds and length (Å)
Anti-inflammatory studies			
FD1		LEU162 (4.21)	LEU162(4.53), TYR166(4.45), ILE232(4.22), PRO410(3.98)

	<div><p>Interactions</p><div><div>van der Waals</div><div>Conventional Hydrogen Bond</div><div>Alkyl</div><div>Pi-Alkyl</div></div></div>		
FD4	<div><p>Interactions</p><div><div>van der Waals</div><div>Alkyl</div><div>Pi-Alkyl</div></div></div>	NON	HIS520(4.61, 4.41), ILE519(4.86), PRO410(4.74), ILE232(3.94, 4.37)
OD5	<div><p>Interactions</p><div><div>van der Waals</div><div>Alkyl</div><div>Pi-Alkyl</div></div></div>	NON	ILE232(4.66, 4.93, 4.92), PRO410(4.41)

	<p>Interactions</p> <ul style="list-style-type: none">van der WaalsPi-SigmaAlkylPi-Alkyl		
OD7	<p>Interactions</p> <ul style="list-style-type: none">van der WaalsAlkylPi-Alkyl	NON	ILE274(4.75), TYR256(4.91), VAL142(4.15)
ASP	<p>Interactions</p> <ul style="list-style-type: none">van der WaalsConventional Hydrogen BondPi-SigmaPi-Alkyl	THR167(3.23), ARG165(4.54, 3.50, 3.55)	ILE232 (5.39), PRO410(5.59)

Antioxidant studies

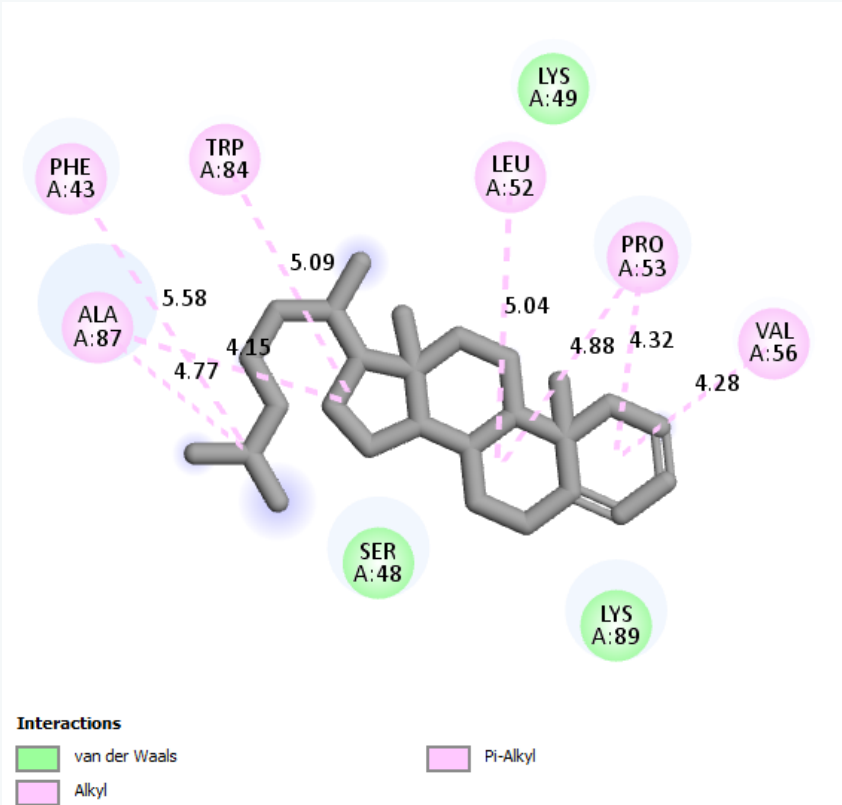
FD1



GLY146(4.26)

VAL39(4.81)

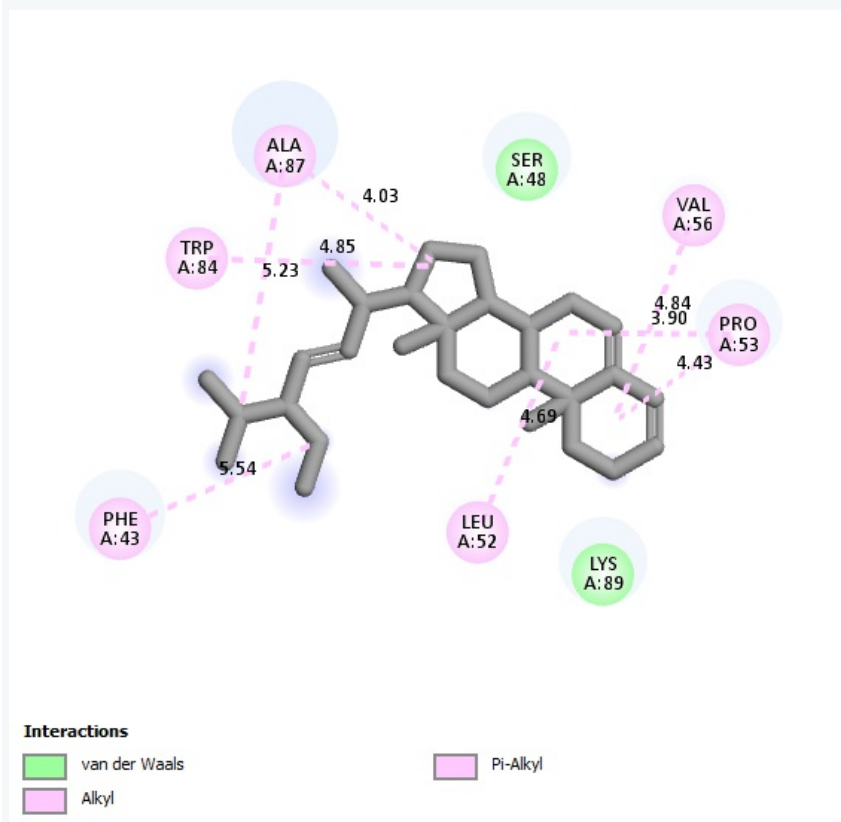
FD4



NON

ALA87(4.15, 4.77),
PRO53(4.32, 4.88),
VAL56(4.28)

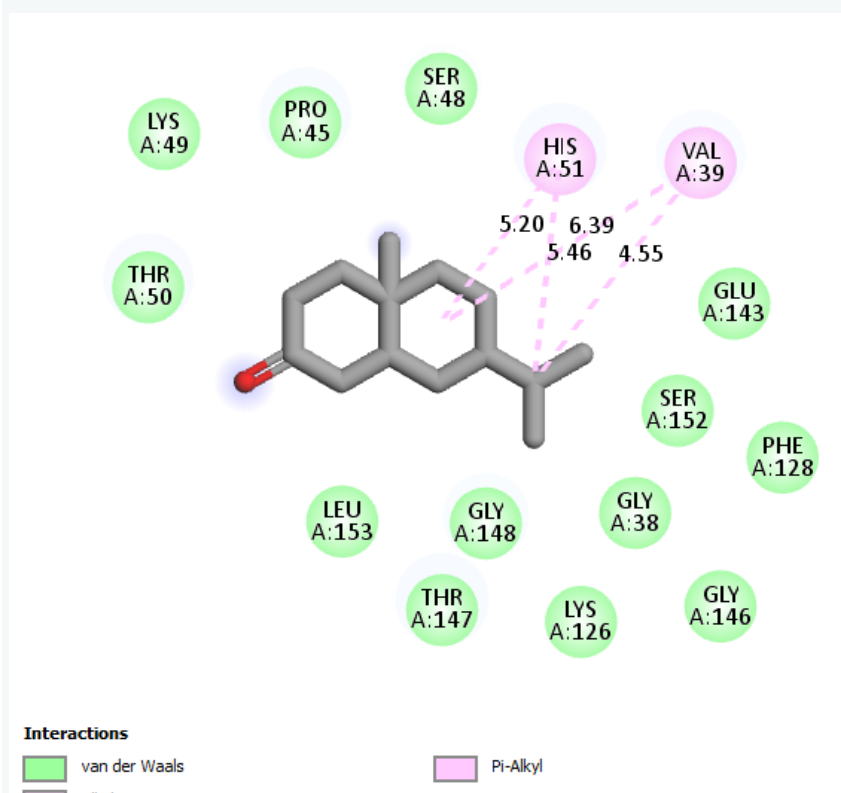
OD5



NON

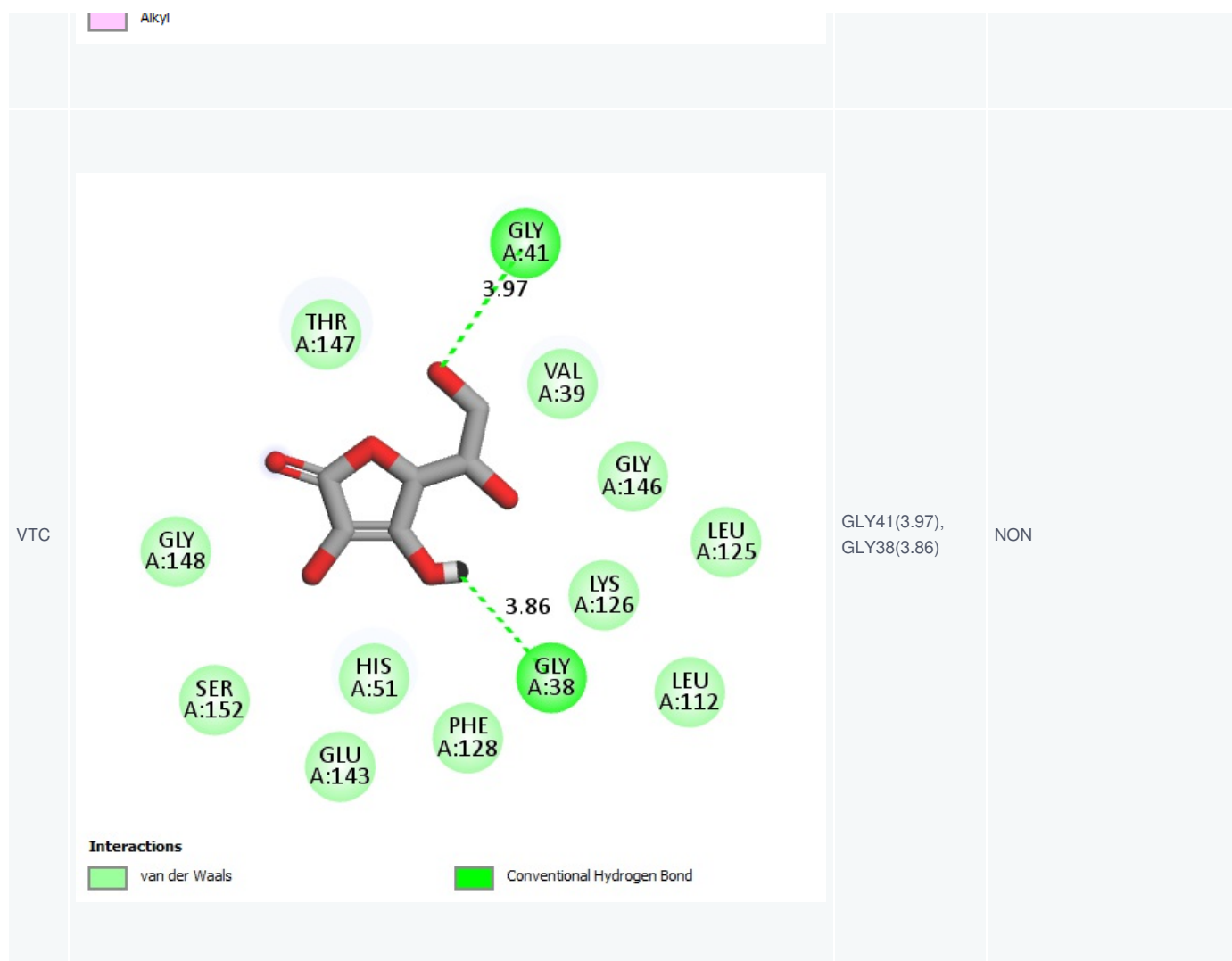
TRP84(4.85), ALA87(4.03),
LEU52(4.69), PRO53(3.90,
4.43)

OD7



NON

VAL39(4.55)



3.5. ADMET studies

Table 4 summarizes the findings of the Absorption Distribution Metabolism Excretion and Toxicity (ADMET) study. Previous studies, such as Falade et al., and de Souza Neto et al., [24][25], have suggested a range of acceptable results for ADMET property studies. Using SMILE formula notations, Xiong et al. [21] and Kiefer et al. [26] successfully trained supervised models to predict the ADMET properties of compounds.

From Table 4, all intestinal absorption results for all qualified compounds are seen to be > 90%. FD-5, FD-6, OD-2, and OD-6 are predicted to be very water soluble. FD-1, FD-3, FD-4, OD-5 and OD-7 are predicted to be fairly soluble. While, OD-3, OD-8 and OD-9 are predicted to be non-soluble in water.

The predicted drug distribution of each of the compounds is predicted to be Negative for all qualified compounds except OD-8. Likewise the metabolism pathway of all compound is predicted to fall in between inhibiting non (0/5) of the cytochrome P450 to inhibit two (2/5) of cytochrome P450 receptors. The half life (T_{1/2}) prediction of the qualified compounds increases from, FD-6 (0.051) < FD-5 (0.063) < FD-4 (0.560) < FD-3 (0.610) < FD-1 (0.73) for freeze-dried ginger. For the oven-dried ginger, half-life increases in the order of OD-6 (0.045) < OD-9 & OD-10 (0.05) OD-2 (0.064) <

OD-8 (0.584) < OD-5 (0.610) < OD-7 (0.628) < OD-3 (0.763).

The Human Either a-go-go ion blocker is predicted to be inactive for FD-1, FD-3, FD-4, OD-3, OD-5, OD-7, and OD-8 while FD-5, FD-6, OD-2, OD-6, OD-9 and OD-10 are predicted to be active.

Table 4. ADMET property prediction to further screen the docking-qualified compounds.							
Compounds	Absorption		Distribution	Metabolism	Excretion	Toxicity	
	HIA	Log S	BBB	CYP 450 inhibition	Half – life (T _{1/2})	hERG blockers	RAT-Toxicity
Freeze-Dried Ginger							
FD-1	> 90%	- 4.622	Negative	0/5	0.73	Inactive	Low
	Good	Soluble			Long		
FD-3	> 90%	-5.223	Negative	0/5	0.610	Inactive	Low
	Good	Soluble			Long		
FD-4	> 90%	-5.721	Negative	0/5	Long	Inactive	Low
	Good	Soluble			0.560		
FD-5	> 90%	-7.280	Negative	0/5	0.063	Active	Low
	Good	Very Soluble			Short		
FD-6	> 90%	-7.611	Negative	1/5	0.051	Active	Low
	Good	Very Soluble			Short		
Oven-Dried Ginger							
OD-2	> 90%	-7.299	Negative	1/5	0.064	Active	Low
	Good	Very Soluble			Short		
OD-3	> 90%	-2.479	Negative	2/5	0.763	Inactive	Low
	Good	Not Soluble			Long		
OD-5	> 90%	-5.223	Negative	0/5	0.610	Inactive	Low
	Good	Soluble			Long		
OD-6	> 90%	-7.218	Negative	2/5	0.045	Active	Low
	Good	Very Soluble			Short		

OD-7	> 90%	-5.230	Negative	0/5	0.628	Inactive	Low
	Good	Soluble			Long		
OD-8	> 90%	-3.414	Positive	0/5	0.584	Inactive	Low
	Good	Not Soluble			Long		
OD-9	> 90%	-6.773	Negative	0/5	0.050	Active	Low
	Good	Very Soluble			Short		
OD-10	> 90%	-6.773	Negative	0/5	0.050	Active	Low
	Good	Very Soluble			Short		

3.6. Protein-ligand complex stability and conformational flexibility by Molecular Dynamics simulations

3.6.1. Root Mean Square Deviation (RMSD) analysis

The RMSD values can help to understand the impact of ligand in a protein-ligand complex regarding the stability or energy minimization of the solvated model.

Table 5. Mean values of Root Mean Square Deviation formed by 3MNG-ligand and 6NPY-ligand complexes over 100ns of simulation time \pm SD.

RMSD (Å)						
Ligands	FD1	FD4	OD5	OD7	VTC	ASP
3MNG	1.502 \pm 0.2059	1.637 \pm 0.3013	1.536 \pm 0.2858	1.375 \pm 0.2381	1.637 \pm 0.3013	
6NPY	1.814 \pm 0.3162	1.806 \pm 0.303	1.673 \pm 0.2897	1.735 \pm 0.3687		2.079 \pm 0.4924

The mean value of each RMSD is presented with the standard deviation (\pm SD). According to Table 5 and Figure 4, the order of average stability brought about by the ligand to the 3MNG-ligand complex (antioxidant study) ranks from FD4 (1.637 \pm 0.3013 Å) < VTC (1.61 \pm 0.275 Å) < OD5 (1.536 \pm 0.2858 Å) < FD1 (1.502 \pm 0.2059 Å) < OD7 (1.375 \pm 0.2381 Å) in an increasing order. For the 6NPY-ligand complex (anti-inflammatory study), the increasing order of stability goes from ASP (2.079 \pm 0.4924 Å) < FD1 (1.814 \pm 0.3162 Å) < FD4 (1.806 \pm 0.303 Å) < OD7 (1.735 \pm 0.3687 Å) < OD5 (1.673 \pm 0.2897 Å).

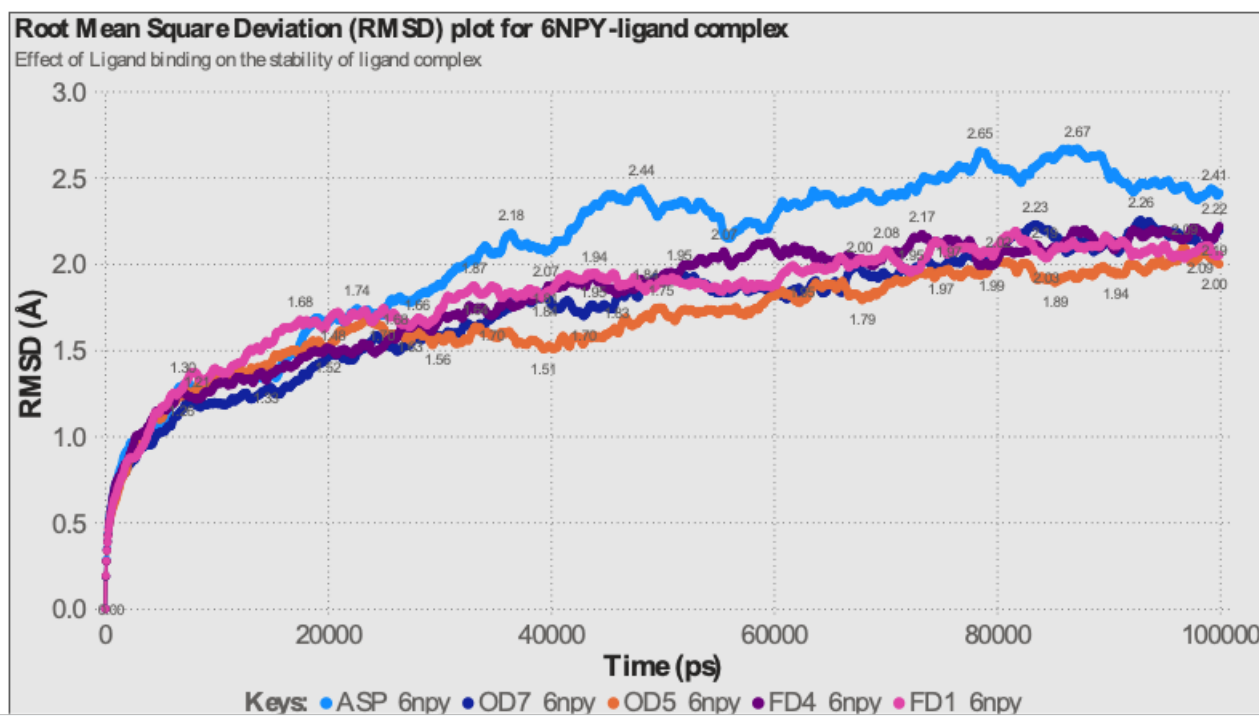
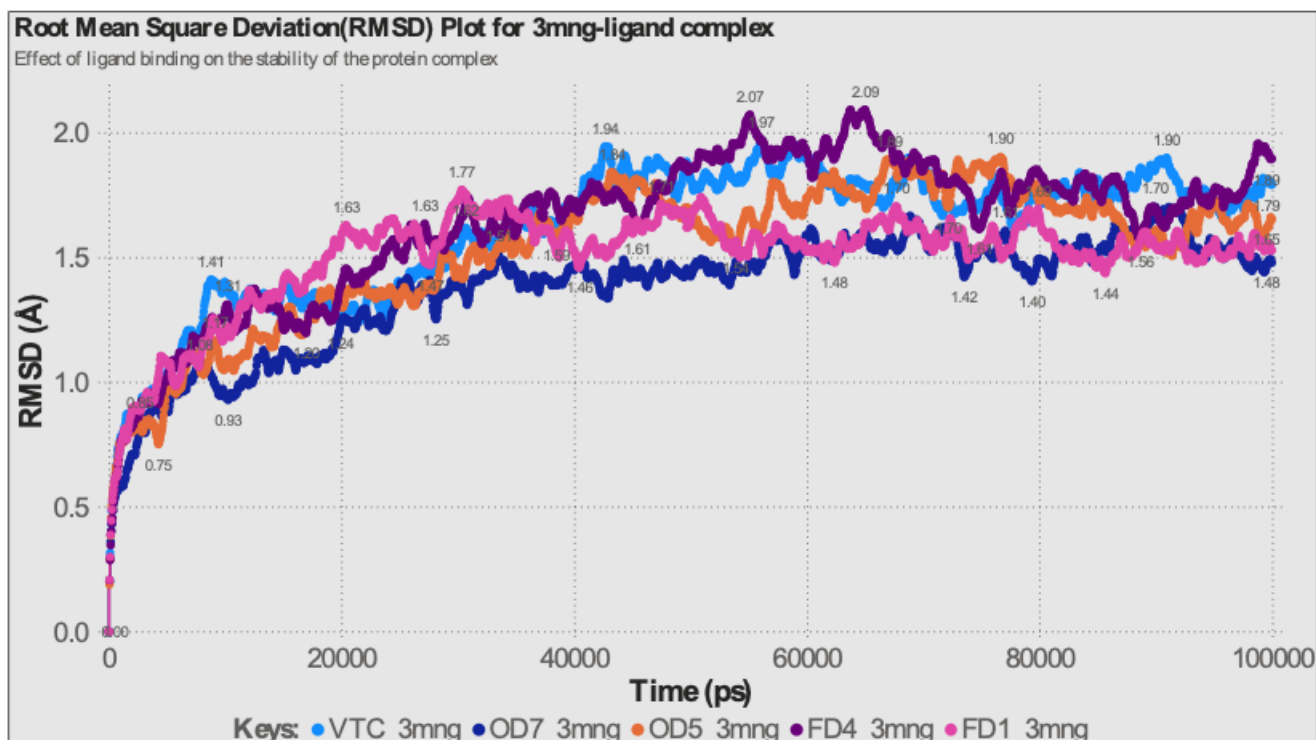


Figure 4. Root Mean Square Deviation (RMSD) plot of 3MNG-ligand (1st frame) and 6NPY-ligand (2nd frame) complexes at 100ns of simulation time. Color index: ASP (maya-blue), FD1 (magenta), FD4 (brown), OD5 (orange), OD7 (blue).

3.6.2. Root Mean Square Fluctuation (RMSF) analysis

The RMSF can help to notice the local changes within the protein backbone structure, which is an effect of the ligand that has binded to it. In reference to Figure 5, shows the conformational changes brought about by the ligands on the RMSF of the protein-ligand complex. Result show that both the regions of hydrogen bond and hydrophobic interactions eg., for

3MNG: GLY 146, TRP84, ALA87, LEU52, and PRO53 all show minimal fluctuation. Similarly, for 6NPY-lignad complex, its binding regions such as LEU162, THR167, ARG165, and ILE232 also show minimal fluctuation.

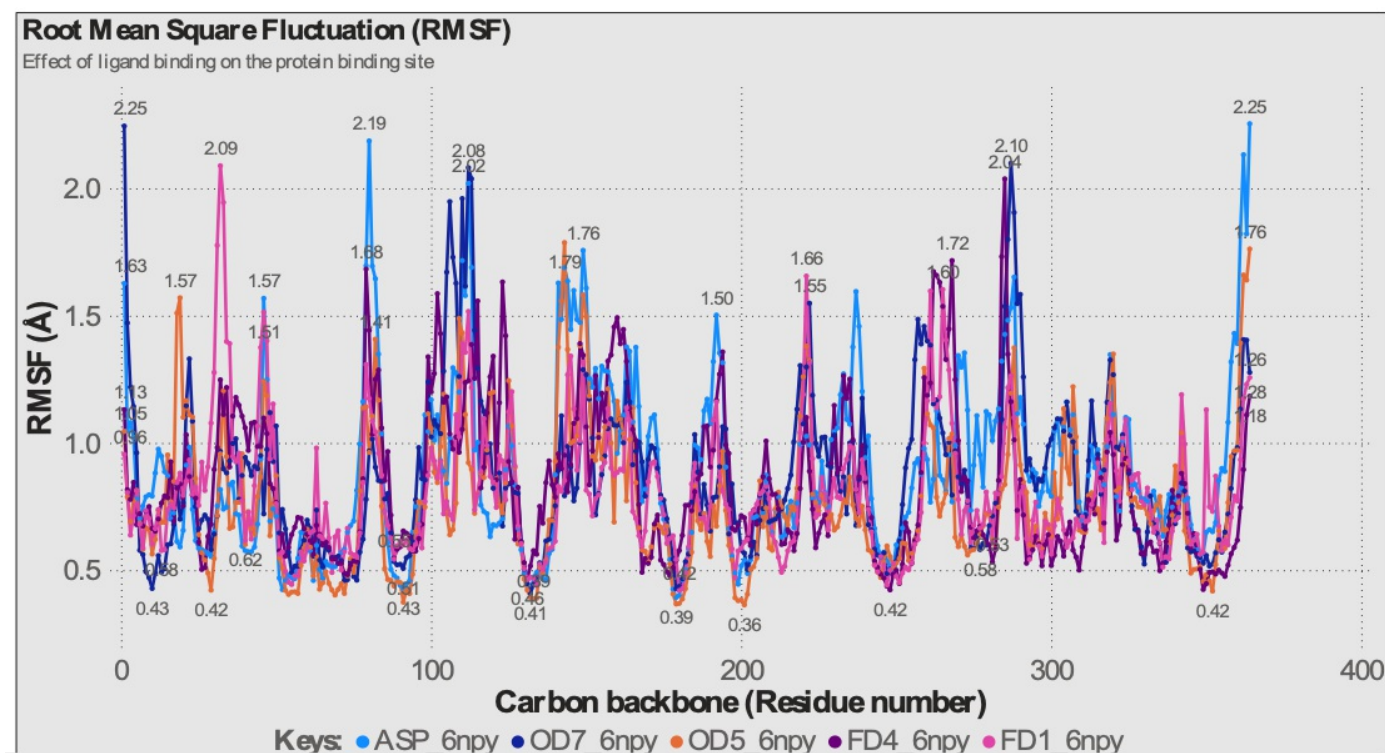
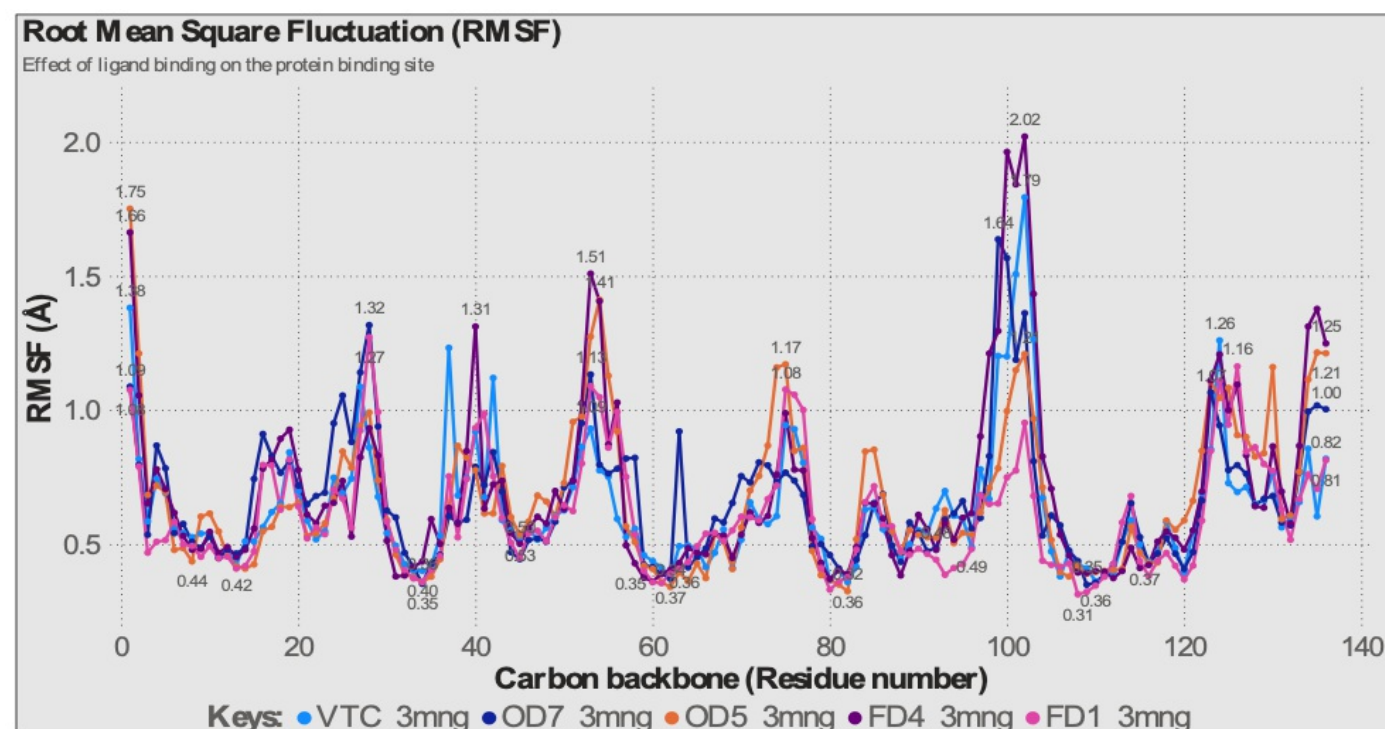


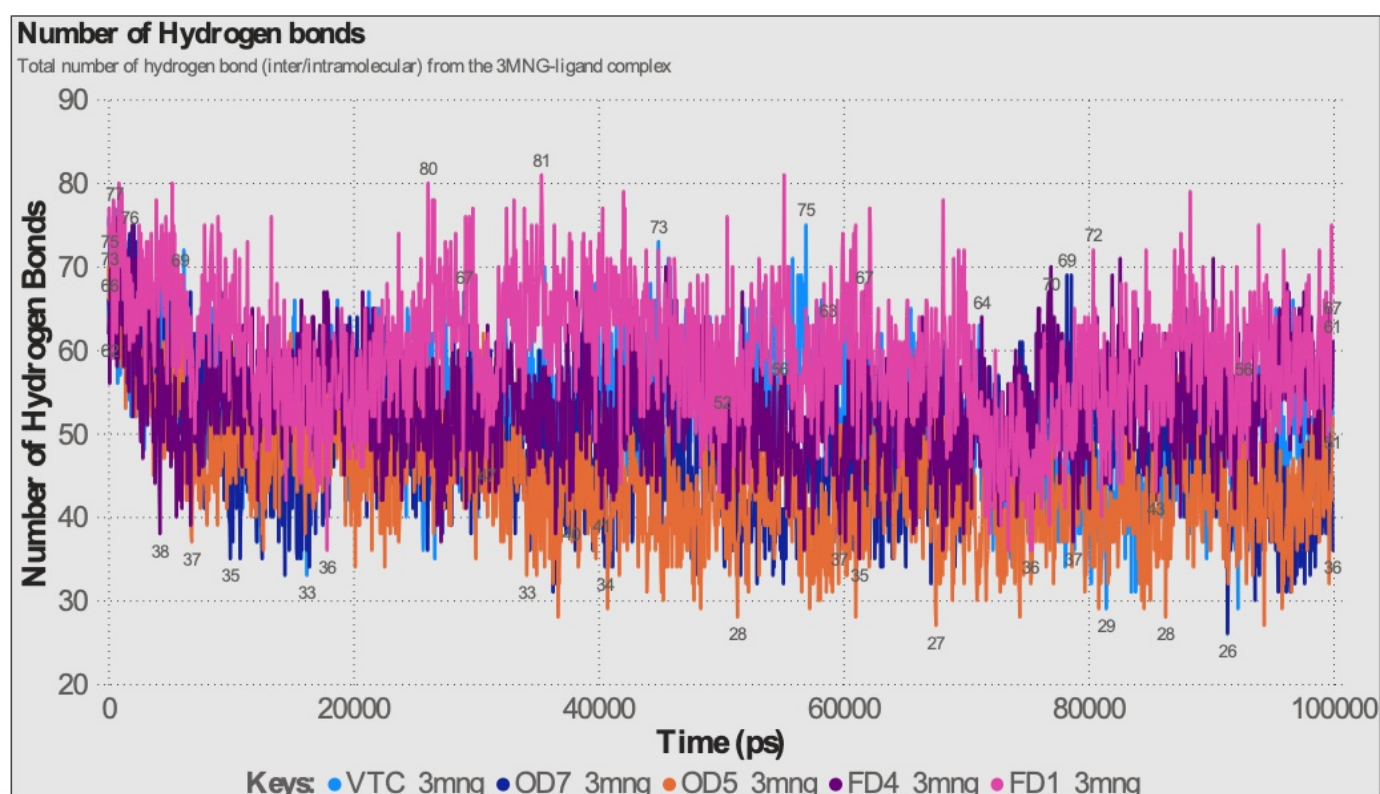
Figure 5. Root Mean Square Fluctuation (RMSF) plot of 3MNG-ligand (1st frame) and 6NPY-ligand (2nd frame) complexes at 100ns of simulation time. Color index: ASP (maya-blue), FD1 (magenta), FD4 (brown), OD5 (orange), OD7 (blue).

3.6.3. Number of Hydrogen Bonds

The number of hydrogen bonds can help in the understanding of a potential drug' drug specificity, metabolism and adsorption properties earlier predicted in the ADMET analysis. Hence, the number of hydrogen bond formed over 100 ns of simulation time, of FD1, FD4, OD5, OD7 VTC and ASP with antioxidant and anti-inflammatory studies, respectively, are as shown in Figure 6. For the ligands bound to the 3MNG protein, Table 6 show that FD1 (59.38 ± 7.455) formed more hydrogen bonds with the 3MNG protein than FD4 (53.8 ± 6.108), VTC (51.61 ± 7.48), OD7 (47.95 ± 7.577) and OD5 (44.3 ± 7.129). For ligands bound to the 6NPY protein, Table 6 show that ASP (158.5 ± 14.82) formed the most hydrogen bond with the protein followed by OD5 (158.5 ± 14.82), FD1 (150.3 ± 14.39), OD7 (149.8 ± 14.49), and FD4 (147.3 ± 13.37).

Table 6. Mean values of Number of hydrogen bonds formed by 3MNG-ligand and 6NPY-ligand complexes over 100ns of simulation time \pm SD.

Number of Hydrogen Bonds						
	FD1	FD4	OD5	OD7	VTC	ASP
3MNG	59.38 ± 7.455	53.8 ± 6.108	44.3 ± 7.129	47.95 ± 7.577	51.61 ± 7.48	
6NPY	150.3 ± 14.39	147.3 ± 13.37	152.5 ± 15.29	149.8 ± 14.49		158.5 ± 14.82



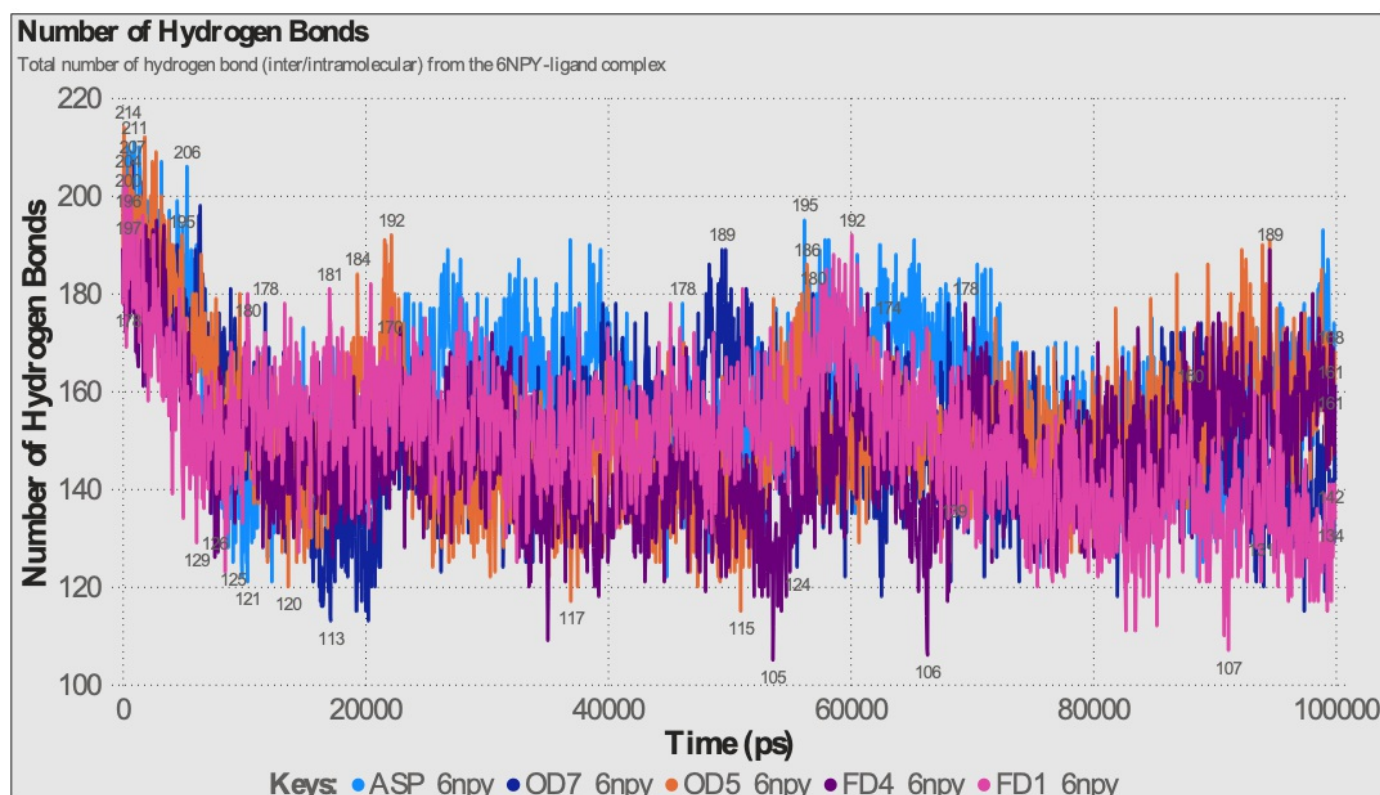


Figure 6. Number of hydrogen bonds plot of 3MNG-ligand (1st frame) and 6NPY-ligand (2nd frame) complexes at 100ns of simulation time. Color index: ASP (maya-blue), FD1 (magenta), FD4 (brown), OD5 (orange), OD7 (blue).

3.6.4. Radius of Gyration (RoG)

The radius of gyration (RoG) is a useful tool since it offers a simple and useful measurement of the size, shape, and dynamics of the simulated complex. It's generally described as the measure of compactness of the protein-ligand complex. A higher RoG value show high flexibility, high unbound state with interacting molecules, and less compactness of the protein-ligand complex. On the other hand, a low RoG value could mean less flexibility (high structural stability), bound state (interacting components closely associated with each other), and high compactness.

Figure 7 shows the plot of RoG over 100ns of time, and Table 7 shows the mean values obtained from the plot, data. Results show that, over 100ns of time and of all ligands interacting with the 3MNG protein, OD5 (14.14 ± 0.103) has the highest RoG value followed by OD7 (14.08 ± 0.062), FD4 (14.09 ± 0.068), VTC (13.97 ± 0.044) and FD1 (13.93 ± 0.043). Furthermore, result show that of the ligands bound to 6NPY, ASP (22.17 ± 0.113) has the highest RoG value followed by FD1 (22.02 ± 0.058), FD4 (21.99 ± 0.04), OD5 (21.98 ± 0.093) and OD7 (21.86 ± 0.081).

Table 7. Mean values of Radius of gyration formed by 3MNG-ligand and 6NPY-ligand complexes over 100ns of simulation time \pm SD.

Radius of gyration (Å)						
	FD1	FD4	OD5	OD7	VTC	ASP
3MNG	13.93±0.043	14.09±0.068	14.14±0.103	14.08±0.062	13.97±0.044	
6NPY	22.02±0.058	21.99±0.04	21.98±0.093	21.86±0.081		22.17±0.113

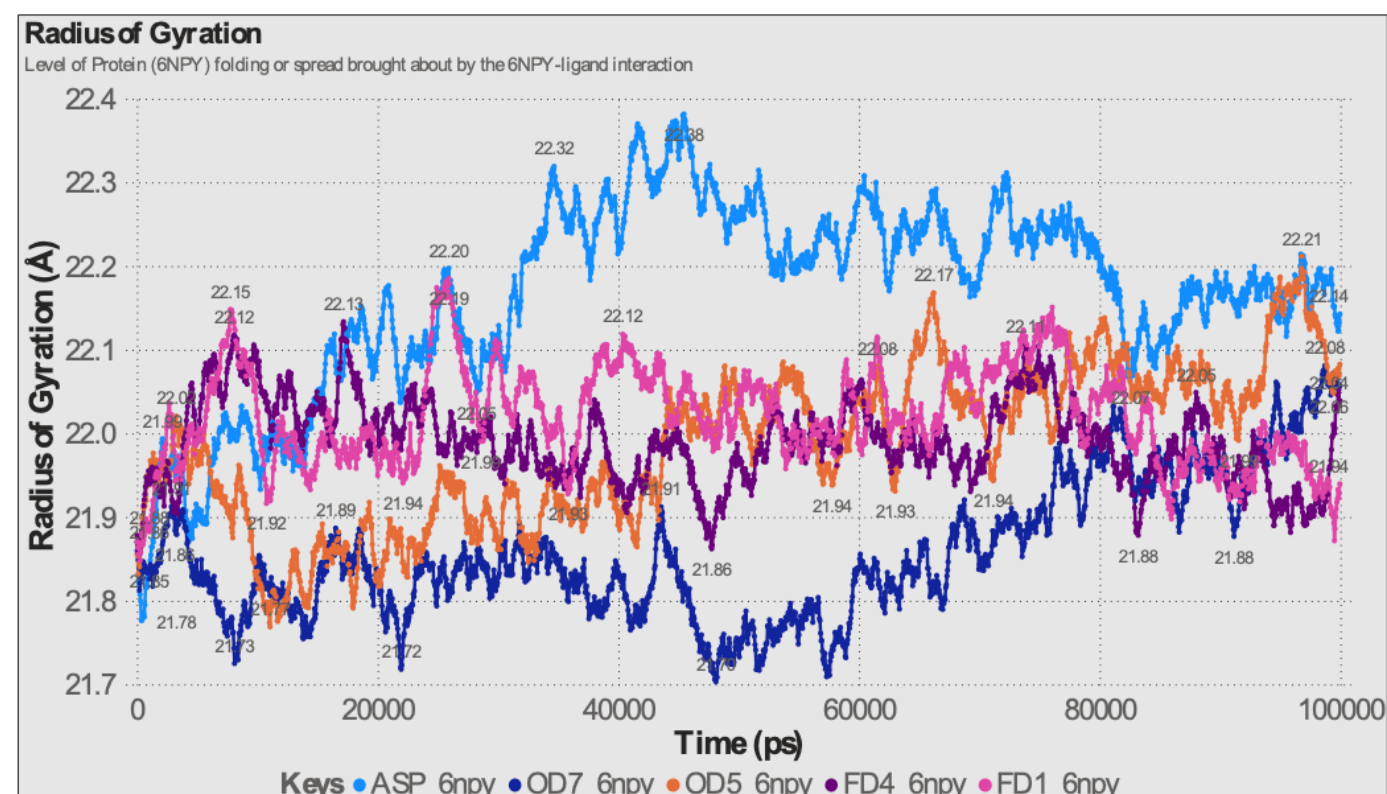
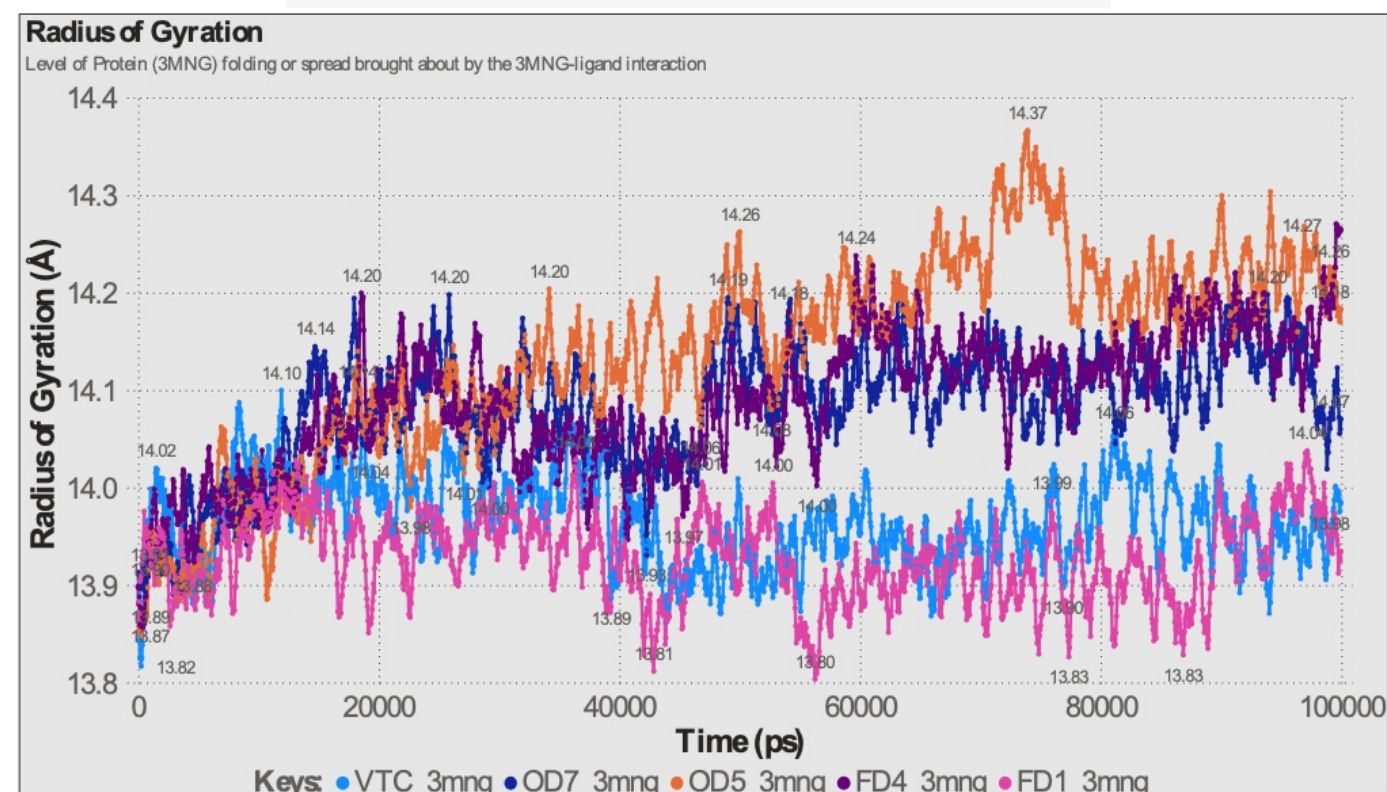


Figure 7. Radius of Gyration (RoG) plot of 3MNG-ligand (1st frame) and 6NPY-ligand (2nd frame) complexes at 100ns of simulation time. Color index: ASP (maya-blue), FD1 (magenta), FD4 (brown), OD5 (orange), OD7 (blue).

3.6.5. Solvent Accessible Surface Area (SASA)

The SASA is useful in monitoring the protein-ligand interaction with the solvent model and helps to ascertain the metabolic pathway of a potential drug. A high SASA region along a simulation period could mean that the ligand as started to free-up it's close interaction with the protein core following its interaction with the solvent and could act as a non-competitive inhibitor. A lower SASA region could mean that the ligand is buried within the protein core and hence, interacts less with the solvent and could act as a competitive inhibitor.

Figure 8 shows the plot of SASA over 100ns of time, and Table 8 shows the mean values obtained from the plotted, data. Results show that all ligands maintained an almost stable SASA value across the simulation period (Table 8). The 3MNG ligands show lower SASA values with values within 7500 – 8500 Å across the 100ns time while the ligands bound to 6NPY receptor showed higher SASA values within 21,000 – 23,000 Å across 100ns of simulated time.

Table 8. Mean values of Solvent Accessible Surface Area (SASA) formed by 3MNG-ligand and 6NPY-ligand complexes over 100ns of simulation time \pm SD.

SASA (Å ²)						
	FD1	FD4	OD5	OD7	VTC	ASP
3MNG	7831 \pm 85.96	8030 \pm 191.1	8240 \pm 268.5	8161 \pm 173.2	7861 \pm 125.2	
6NPY	21910 \pm 198.6	22180 \pm 231.8	22230 \pm 374.8	21940 \pm 245.3		22030 \pm 237.5

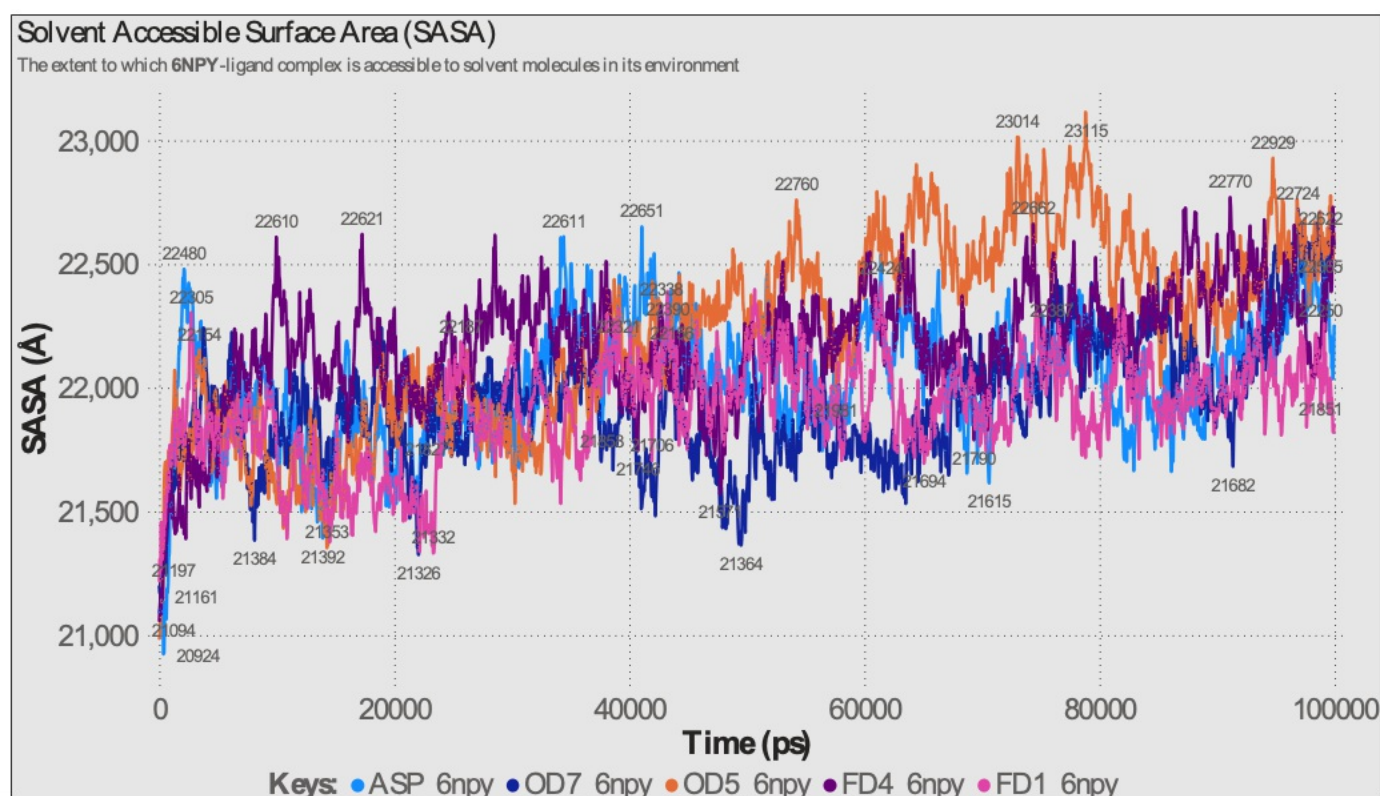
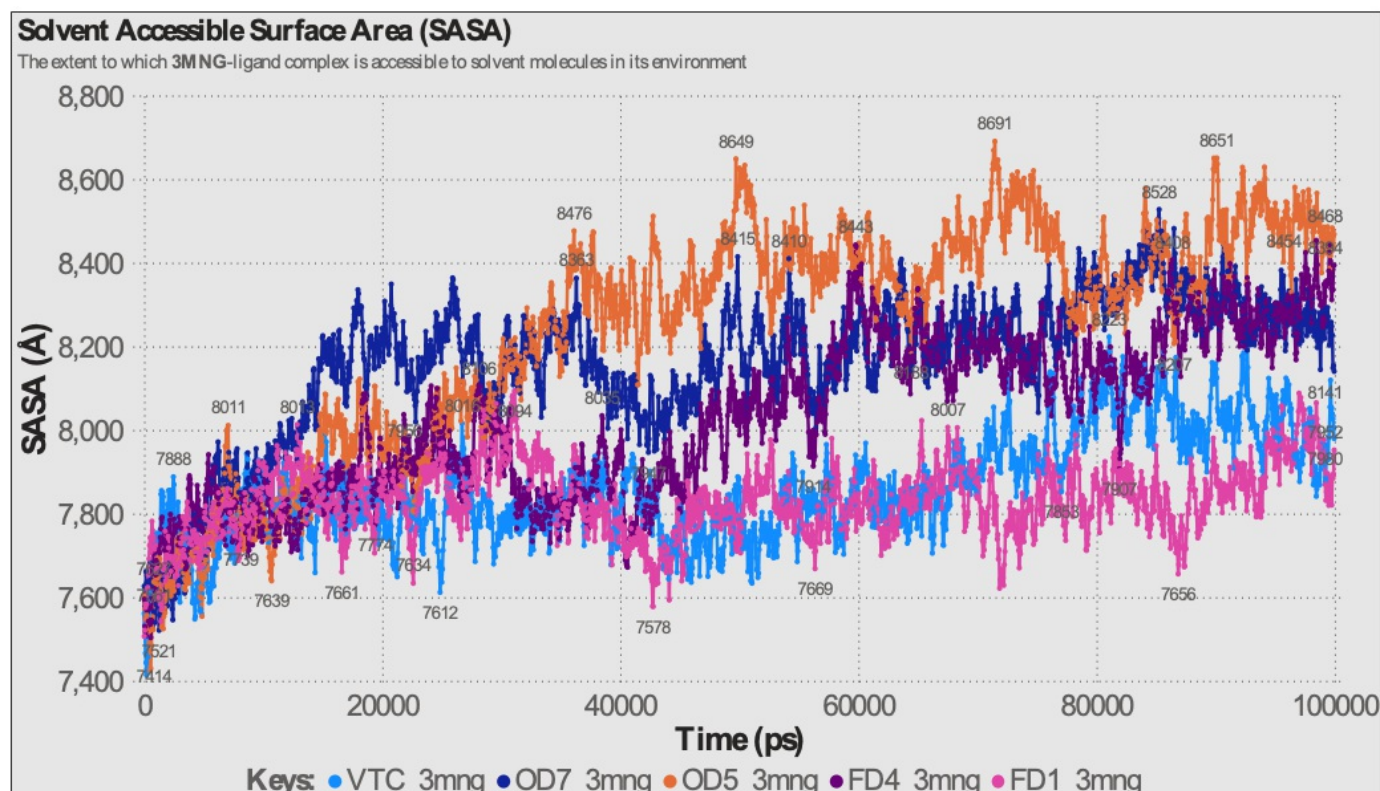


Figure 8. Solvent Accessible Surface Area (SASA) plot of 3MNG-ligand (1st frame) and 6NPY-ligand (2nd frame) complexes at 100ns of simulation time. Color index: ASP (maya-blue), FD1 (magenta), FD4 (brown), OD5 (orange), OD7 (blue).

4. Discussions

The similarities in specific peaks across all extracts in the GCMS plots for oven- and freeze-dried ginger, are due to the fact that these compounds are reasonably stable during the drying processes (Supplementary Data 2). It is noteworthy that the presence of predominant peaks in oven- and freeze-dried ginger but not in raw ginger suggests the concentration of particular compounds during the drying processes. Vaporization, thermal dissociation, and the preservation of volatile compounds are a few cases that could have caused these variations [27].

Phenolics and flavonoids have been reported to contain anti-inflammatory and antioxidant properties [7]. Results from Figure 1 and Supplementary Data 3 confirm and agree with previous studies [15] that both FD-G and OD-G possess more anti-inflammatory and antioxidant properties than RW-G.

In order to gain more in vitro knowledge about which of the drying methods possess more anti-inflammatory or antioxidant properties than the other, scavenging activity analyses were performed. Results according to Figure 2 and Supplementary Data 3 show that FD-G has more antioxidant activity (DPPH radical quenching activity and ABTS scavenging activity) compared to OD-G and RW-G, while OD-G has more anti-inflammatory activities (Nitric oxide scavenging activity and Albumin denaturation) compared to FD-G and RW-G.

While the in vitro results above are in line with the findings of [7] the major intervention of this study begins at the point of investigating, in silico, first, the Protein-ligand interactions via molecular docking study in order to narrow down or screen the ligands or compounds predominantly contained in the raw, oven-, and freeze-dried ginger samples to potential ligands that can be seen to be most responsible for the anti-inflammatory and antioxidant activity of ginger. Vitamin C, or Ascorbic acid, and Aspirin® are the selected standard drugs for comparative analysis in the in silico section of this study. Furthermore, peroxidoxin V (PrxV), represented by PDB ID 3MNG, was the protein used for the antioxidant study, while the NLRP3 inflammasome, represented by PDB ID 6NPY, was the protein used for the anti-inflammatory studies.

Results from Table 2 and Figure 3 reveal how both FD-G and OD-G ligands perform better than the RW-G ligands. This could infer that, truly, the anti-inflammatory and antioxidant activities of ginger are improved upon drying. Ligands such as FD-1, FD-3, FD-4, FD-5, FD-6, OD-2, OD-3, OD-5, OD-6, OD-7, OD-8, OD-9, and OD-10 all scored better binding affinity to both the 3MNG and 6NPY proteins.

The aim of the ADMET study was to predict the qualified ginger ligands' toxicity, distribution, metabolism, and excretion patterns from the molecular docking study. Results from Table 4 revealed that most compounds had good intestinal absorption (>90%) and were expected to be very or moderately water-soluble. According to these ligands' metabolic routes, cytochrome P450 receptors are only mildly inhibited. Ligands such as FD-1, FD-3, FD-4, OD-5, and OD-7 are seen to satisfy the ADME and Toxicity requirements of a potential drug, as reported by [22], [24]. Additionally, the anticipated half-life (T_{1/2}) values demonstrated the eligible compounds' stability and possible treatment duration. The binding interactions of these ligands are described in Table 3, showing how FD1 and the standard drugs VTC and ASP interact via hydrogen bonding and hydrophobic interactions, while FD4, OD-5, and OD-7 do not interact via hydrogen bonding with the protein but with hydrophobic interactions.

Complex stability and conformational flexibility of the protein-ligand complex are needed to understand the behavior of the

other ligands that didn't interact via hydrogen bonding but have better affinity for the protein than the standard drugs that interact via hydrogen bonds.

RMSD results show that the interaction of OD-7 and FD-1 with the protein-ligand complex of 3MNG helps stabilize the complex by up to 16.0% and 8.24%, respectively, from the mean stabilization position of VTC (1.637Å) and also that OD-5 and OD-7 bound to the protein-ligand complex of 6NPY help stabilize the complex by 19.5% and 16.5%, respectively, from the mean stabilization value of ASP (2.079Å). This result infers that OD-7, OD-5, and FD-1 are the most contributing ligands or compounds to the anti-inflammatory and antioxidant properties of ginger by virtue of their stabilization energy potentials.

RMSF analysis shown in Figure 5 infers that binding regions such as GLY 146, TRP84, ALA87, LEU52, and PRO53 for the 3MNG-ligand complex and LEU162, THR167, ARG165, and ILE232 for the 6NPY-ligand complex show minimum fluctuations for FD-1, OD-7, and OD-5 ligands in protein complexes, while FD-4, VTC, and ASP offer larger fluctuations in their complex structure. Hence, the mentioned ligands excelled in offering stability to their complex structures.

For the number of hydrogen bonds formed with 3MNG protein, results show that FD1 formed the most H-bonds with the protein, which correlates with the earlier result statements about 3MNG-FD-1 interaction. The result further points to the high number of hydrogen bonds formed for ASP, OD5, FD1, and OD7 with the 6NPY protein. From the introduction of force fields to the conformational flexibility of both ligand and water-mediated hydrogen bonds, the presence of hydrogen bonds for OD5 and OD7 that were absent in the molecular docking study is explained. This could also point out the extra significance that Molecular Dynamics studies offer over molecular docking studies only.

To confirm the above results regarding the expected compactness of the protein complex measured by the Radius of Gyration, RoG, FD-1 formed the most compact shape (less flexibility) with the 3MNG protein, while the OD-5 and OD-7 ligands formed a loose shape or unbound state. This could be a good reason why the molecular docking studies could not locate their interactions via hydrogen bonding because of the unbound shape they formed with the protein structure. A confirmation is that FD1 shows the lowest SASA value with 3MNG (7831Å²) and with 6NPY (21910Å²) which means that FD-1 conforms closer to the protein core and could likely act as a competitive inhibitor.

Although further studies are needed to isolate FD-1, OD-5, and OD-7 for in vivo validity analysis, this study is able to establish the fact that (E)-octadec-9-enoic acid (FD1), Stigmastan-3,5,22-trien (OD-5), and octahydro-4a-methyl-7-(1-methylethyl)-2(1H)-Naphthalenone (OD-7) are the potential compounds that are responsible for the anti-inflammatory and antioxidant properties of ginger. Also, it had been established that the oven-drying followed by the freeze-drying methods would greatly increase the yield of isolating this bioactive components from ginger.

5. Conclusions

The purpose of this study was to pinpoint the precise component or compounds in ginger (*Zingiber officinale* Roscoe) that are responsible for its anti-inflammatory and antioxidant effects. The study has offered useful insights through a thorough

analysis involving metabolic processes, genetic receptor interactions, toxicity screening, and molecular dynamics studies. It was confirmed that phenolics and flavonoids had considerable anti-inflammatory and antioxidant activities. Additionally, it was discovered that oven-dried ginger (OD-G) had more potent anti-inflammatory effects than freeze-dried ginger (FD-G), which also showed higher antioxidant activity. (E)-octadec-9-enoic acid (FD1), Stigmastan-3,5,22-trien (OD-5), and octahydro-4a-methyl-7-(1-methylethyl)-2(1H)-Naphthalenone (OD-7) were the ligands that contributed most to ginger's antioxidant and anti-inflammatory activity, according to in silico studies. With FD-1, OD-5, and OD-7 as viable candidates, these study open the door for the prospective development of effective anti-inflammatory and antioxidant medications. The findings generally indicate that dried ginger has the potential to increase ginger's anti-inflammatory and antioxidant activity by 12.90 – 17.91% and 4 – 11.2%, respectively, compared to raw ginger. However, the specific bio-efficiency of dried ginger would be greatly influenced by the drying technique employed. Further in vivo studies are essential to validate and harness the full medicinal potential of ginger and the effectiveness of drying options on its bio-activities.

Statements and Declarations

Research funding

This research did not receive any specific grant from funding agencies in the public, commercial or non-profit sectors.

Conflict of Interest

The authors declare that they have no competing interest

Other References

- W. Humphrey, A. Dalke, and K. Schulten, "VMD: visual molecular dynamics," J. Mol. Graph., vol. 14, no. 1, pp. 33–38, 1996, doi: 10.1155/2020/8811597.
- M. T. Nelson et al., "NAMD: a parallel, object-oriented molecular dynamics program," Int. J. Supercomput. Appl. High Perform. Comput., vol. 10, no. 4, pp. 251–268, 1996.
- S. H. Nile and S. W. Park, "Chromatographic analysis, antioxidant, anti-inflammatory, and xanthine oxidase inhibitory activities of ginger extracts and its reference compounds," Ind. Crops Prod., vol. 70, pp. 238–244, 2015, doi: 10.1016/j.indcrop.2015.03.033.
- D. Laveti et al., "Anti-inflammatory treatments for chronic diseases: a review," Inflamm. Allergy-Drug Targets (Formerly Curr. Drug Targets-Inflammation Allergy) (Discontinued), vol. 12, no. 5, pp. 349–361, 2013, doi: 10.2174/18715281113129990053.

References

1. ^{a, b}O. Ekundayo, I. Laakso, and R. Hiltunen, "Composition of ginger (*Zingiber officinale* Roscoe) volatile oils from Nigeria," *Flavour Fragr. J.*, vol. 3, no. 2, pp. 85–90, 1988, doi: 10.1002/ffj.2730030207.
2. [^]M. I. Kazeem, M. A. Akanji, R. M. Hafizur, and M. I. Choudhary, "Antiglycation, antioxidant and toxicological potential of polyphenol extracts of alligator pepper, ginger and nutmeg from Nigeria," *Asian Pac. J. Trop. Biomed.*, vol. 2, no. 9, pp. 727–732, 2012.
3. ^{a, b}Y. P. Lim, S. F. Pang, M. M. Yusoff, and J. Gimbut, "Correlation between the antioxidant, total flavonoid and total phenolic content of *Phaleria macrocarpa* fruit extract," *IJRTE*, vol. 8, pp. 38–42, 2019, doi: 10.1016/j.jarmap.2019.100224.
4. [^]E. Jayashree, R. Visvanathan, and J. Zachariah, "Quality of dry ginger (*Zingiber officinale*) by different drying methods," *J. Food Sci. Technol.*, vol. 51, no. 11, p. 3190, 2014, doi: 10.1007/s13197-012-0823-8.
5. [^]A. V Famurewa, P. O. Emuekele, and K. F. Jaiyeoba, "Effect of drying and size reduction on the chemical and volatile oil contents of ginger (*Zingiber officinale*)," *J. Med. Plants Res.*, vol. 5, no. 14, pp. 2941–2944, 2011.
6. [^]G. I. Okafor and J. N. C. Okafor, "Effects of pricking, sun-drying and sieving on Ginger (*Zingiber officinale* Roscoe) colour and powder," 2007, doi: 10.4314/nifo.v25i1.33664.
7. ^{a, b, c, d}I. Mustafa, N. L. Chin, S. Fakurazi, and A. Palanisamy, "Comparison of phytochemicals, antioxidant and anti-inflammatory properties of sun-, oven- And freeze-dried ginger extracts," *Foods*, vol. 8, no. 10, 2019, doi: 10.3390/foods8100456.
8. [^]K. An, D. Zhao, Z. Wang, J. Wu, Y. Xu, and G. Xiao, "Comparison of different drying methods on Chinese ginger (*Zingiber officinale* Roscoe): Changes in volatiles, chemical profile, antioxidant properties, and microstructure," *Food Chem.*, vol. 197, pp. 1292–1300, 2016, doi: 10.1016/j.foodchem.2015.11.033.
9. ^{a, b}T. T. Mutukuri, N. E. Wilson, L. S. Taylor, E. M. Topp, and Q. T. Zhou, "Effects of drying method and excipient on the structure and physical stability of protein solids: Freeze drying vs. spray freeze drying," *Int. J. Pharm.*, vol. 594, p. 120169, 2021, doi: 10.1016/j.ijpharm.2020.120169.
10. ^{a, b}S. Shukla, "Freeze drying process: A review," *Int. J. Pharm. Sci. Res.*, vol. 2, no. 12, p. 3061, 2011.
11. ^{a, b}M. Buvaneswaran, N. Venkatachalapathy, A. Rawson, and C. K. Sunil, "Impact of Freeze-drying on physiochemical, structural, and mechanical properties of ginger (*Zingiber officinale*)," *Pharma Innov. J.*, vol. 10, no. 10, pp. 1704–1710, 2021.
12. [^]S. BEYHAN and H. İŞLEROĞLU, "EXTRACTION OF PHENOLIC COMPOUNDS FROM FENUGREEK SEEDS: MODELLING AND ANALYSIS USING ARTIFICIAL NEURAL NETWORKS," *Konya J. Eng. Sci.*, vol. 11, no. 2, pp. 312–323, 2023, doi: 10.36306/konjes.1208658.
13. [^]I. González-Palma et al., "Evaluation of the antioxidant activity of aqueous and methanol extracts of *Pleurotus ostreatus* in different growth stages," *Front. Microbiol.*, vol. 7, p. 1099, 2016, doi: 10.3389/fmicb.2016.01099.
14. [^]S. M. Kaddour, L. Arrar, and A. Baghiani, "Anti-Inflammatory Potential Evaluation (In-Vitro and In-Vivo) of *Arthrophytum scoparium* Aerial Part," *J. Drug Deliv. Ther.*, vol. 10, no. 5, pp. 213–218, 2020, doi: 10.22270/jddt.v10i5.4409.
15. ^{a, b}N. Mills, "ChemDraw Ultra 10.0 CambridgeSoft, 100 CambridgePark Drive, Cambridge, MA 02140. www.cambridgesoft.com. Commercial Price: 1910fordownload, 2150 for CD-ROM; Academic Price: 710fordownload, 800

for CD-ROM." ACS Publications, 2006. doi: 10.1021/ja0697875.

16. ^aN. L. Allinger, Y. H. Yuh, and J. H. Lii, "Molecular mechanics. The MM3 force field for hydrocarbons. 1," *J. Am. Chem. Soc.*, vol. 111, no. 23, pp. 8551–8566, 1989, doi: 10.1002/jcc.540110708.
17. ^aP. W. Rose et al., "The RCSB protein data bank: integrative view of protein, gene and 3D structural information," *Nucleic Acids Res.*, p. gkw1000, 2016.
18. ^aD. S. BIOVIA, "BIOVIA pipeline pilot. Dassault Systèmes: San Diego, BW, Release." 2021.
19. ^aT. D. Goddard, C. C. Huang, and T. E. Ferrin, "Software extensions to UCSF chimera for interactive visualization of large molecular assemblies," *Structure*, vol. 13, no. 3, pp. 473–482, 2005, doi: 10.1016/j.str.2005.01.006.
20. ^aO. Trott and A. J. Olson, "AutoDock Vina: improving the speed and accuracy of docking with a new scoring function, efficient optimization, and multithreading," *J. Comput. Chem.*, vol. 31, no. 2, pp. 455–461, 2010, doi: 10.1002/jcc.21334.
21. ^{a, b}G. Xiong et al., "ADMETlab 2.0: An integrated online platform for accurate and comprehensive predictions of ADMET properties," *Nucleic Acids Res.*, vol. 49, no. W1, pp. W5–W14, 2021, doi: 10.1093/nar/gkab255.
22. ^{a, b, c}Lipinski, "Poor aqueous solubility—an industry wide problem in drug discovery," *Am Pharm Rev*, vol. 5, no. 3, pp. 82–85, 2002.
23. ^aS. Jo, T. Kim, V. G. Iyer, and W. Im, "CHARMM-GUI: a web-based graphical user interface for CHARMM," *J. Comput. Chem.*, vol. 29, no. 11, pp. 1859–1865, 2008, doi: 10.1002/jcc.20945.
24. ^{a, b}V. A. Falade, T. I. Adelusi, I. O. Adedotun, M. Abdul-Hammed, T. A. Lawal, and S. A. Agboluaje, "In silico investigation of saponins and tannins as potential inhibitors of SARS-CoV-2 main protease (Mpro)," *Silico Pharmacol.*, vol. 9, no. 1, 2021, doi: 10.1007/s40203-020-00071-w.
25. ^aL. R. de Souza Neto et al., "In silico Strategies to Support Fragment-to-Lead Optimization in Drug Discovery," *Front. Chem.*, vol. 8, no. February, pp. 1–18, 2020, doi: 10.3389/fchem.2020.00093.
26. ^aF. Kiefer, K. Arnold, M. Künzli, L. Bordoli, and T. Schwede, "The SWISS-MODEL Repository and associated resources," *Nucleic Acids Res.*, vol. 37, no. suppl_1, pp. D387–D392, 2009, doi: 10.1093/nar/gkn750.
27. ^aO. E. Udu-Ibiam et al., "Phytochemical and antioxidant analyses of selected edible mushrooms, ginger and garlic from Ebonyi State, Nigeria," *IOSR J Pharm Biol Sci*, vol. 9, no. 3, pp. 86–91, 2014, doi: 10.9790/3008-09348691.